

SOS-Phase III: EPA Agreement #RD-82897601  
Final Report  
Georgia Institute of Technology  
Atlanta, GA

## 1. Introduction

Georgia Institute of Technology's activities as part of Phase III of the Southern Oxidants Study (SOS) were devoted to four primary activities. The most arduous was the archiving of the Atlanta Supersite data in to the NARSTO Data Base. As noted below, this was an iterative and time consuming effort, requiring significant effort and communication by both the Georgia Tech scientist in charge of this aspect of the project, as well as individuals associated with the NARSTO Data Base. Part of the effort was associated with addressing new issues involved in making Supersite-level data in the correct form for acceptance in the data base. A second activity involved continued development and application of Models 3 components, primarily CMAQ. Application was to the Southeast, in part with application to SOS intensive study periods. Two activities were instrument development-related. Funds from this portion of SOS were used to continue development of both a water soluble PM analyzer and a water insoluble particle analyzer. A major portion of the funds also were used in a subcontract to fund Dr. Richard McNider who coordinated the modeling aspects of SOS. These activities, and the accomplishments, are described below.

## 2. SOS Modeling Coordination

Under the SOS activity, Dr. Richard McNider was employed as a consultant under the SOS Cooperative Agreement to Georgia Tech. Under this arrangement Dr. McNider coordinated SOS physical modeling activities primarily at the University of Alabama in Huntsville. Much of the work involved planning and coordination of SOS modeling activities related to SOS 99 field program activities and TEXAQS2000 field program activities. A summary of these activities are provided below. Some of these activities are covered in the UAH Final Report under UAH's SOS Cooperative Agreement. Also, some of the projects relate to joint activities supported by the Texas Commission on Environmental Quality and EPA STAR Grants. Specific acknowledgements are given for each project.

Five projects are discussed:

1. Application of Coupled LES-Chemistry Model Applied to Industrial Source During TEXAQS2000
2. Role of Deformed Flows in Extreme Concentration Events in the Southeast
3. Meteorological Simulations for 1999 SOS Field Intensive Periods
4. Analysis of Winds Observed by Radar Profilers
5. Development of a Web-Based Lagrangian Particle Model

## **2.1. Application of Coupled LES-Chemistry Model Applied to Industrial Source During TEXAQS2000**

Transient high ozone events (THOEs), defined as rapid ozone ( $O_3$ ) concentration increases and decreases of more than  $50 \text{ ppbv h}^{-1}$  as measured by surface monitors, have been observed downwind of industrial source complexes. THOEs often result in exceedances of the one-hour  $O_3$  NAAQS of 120 ppbv. Typical coarse-grid air quality models are unable to reproduce the rapid  $O_3$  formation or peak values. Complex photochemical scenarios are suspected of yielding non-negligible concentration covariances in the turbulent boundary layer.

### **2.1.1. Goals of the Present Numerical Study**

- Test feasibility of utilizing online coupled large-eddy simulation (LES)-photochemical model as a tool for studying ozone production near industrial sources.
- Start with idealized test cases, conducting simulations for different source scenarios.
- Examine resulting trace gas statistics and concentration covariances for significance.

#### **A-2. ONLINE COUPLED MODEL DESIGN**

The *LESchem* Model (Large-Eddy Simulation with chemistry) was developed by Jerry Herwehe as part of his dissertation research at the University of Alabama in Huntsville. It combines the RAMS regional scale model with the SMVGEARII model developed by Jacobson.

$$\text{RAMS} + \text{SMVGEAR II} = \text{LESchem}$$

**RAMS** is the Regional Atmospheric Modeling System (Pielke *et al.* 1992)

**SMVGEAR II** is the Sparse Matrix Vectorized Gear solver (Jacobson, 1998)

Every coupled time step RAMS sends current  $T$ ,  $p$ , and trace gas distributions to SMVGEAR. SMVGEAR solves photochemical reactions then sends back updated gas distributions. RAMS emits, deposits, transports, and diffuses gases while solving LES dynamics. Steps repeat, marching chemistry and dynamics forward in time together.

NCAR's Tropospheric Ultraviolet and Visible (TUV) model (Madronich and Flocke, 1998) computes the time- and height-dependent photolysis rates (J-values) used by *LESchem*. A pseudo-spherical 8-stream discrete ordinates radiative transfer scheme provides 1% accuracy or better.

### **A-3. Inserting and Testing of Chemical Mechanism**

Prior to carrying out the actual experiments several activities were undertaken. The CB IV chemical mechanism was added to the model. This included testing of model results against box models and testing of photolysis rates.

### **A-4. Procedures for calculating gridded segregation coefficients.**

Code was developed to compute gridded segregation coefficients and other analysis procedures.

## **A-5. Model Runs**

Under this task NOAA ATDD and UAH carried out a set of simulations using LESchem exploring the near-source ozone production from an industrial source. The experiments combined emission scenarios developed for a petrochemical facility in 2000 supplied by the NOAA Aeronomy Laboratory and TNRCC. For one experiment emissions were based on total reactive hydrocarbon for the total facility emissions and were increased based on aircraft measurements. The point-source distribution of emissions was defined based on an analysis of the 1993 episode centered around the upset scenarios in the Houston Ship Channel area. The distribution was provided by Harvey Jeffries and Tom Tesche. This work indicated that large amounts of reactive hydrocarbons might be released simultaneously from a point flare with concurrent NO<sub>x</sub> emissions. A second scenario requested by TNRCC was to use the emissions based on the TNRCC emissions data base in which the hydrocarbon emissions were approximately a factor of ten less than the aircraft-deduced emissions.

The results presented here are hypothetical. They represent emission hydrocarbons and NO<sub>x</sub> representative of NO<sub>x</sub> and hydrocarbon ratios deduced during the TEXAQS period assuming that the NO<sub>x</sub> and HC emissions were released from the same point. The actual emission from the petrochemical facility was probably not a co-located release.

The simulations used the CB-IV chemical mechanism coupled within the RAMS large-eddy simulation (LES) code. The major purpose of these experiments was to examine photochemical production rates within fine-scale LES structure. A key factor in short-term photochemical production is the degree of separation of chemical species resulting from the turbulent structure in the boundary layer. For example, if two species (e.g., NO and ethylene) are emitted separately (by 300 m or more) so that their emissions are emitted into different parts of a large convective eddy, it may take on the order of three to four eddy timescales (of order 45 minutes) for the species to be fully mixed. Such segregation can drastically slow ozone production. Early on, the ozone may be produced in patches where the NO and ethylene do meet. There may be some ozone consumption in the high NO areas, leading to further early patchiness. Gradually, over 30-45 minutes, the ozone plume would fill in as mixing becomes complete.

If two species are co-emitted (at least within the same part of the large eddy structure), the photochemistry can go quite fast since NO and ethylene are mixed quickly. In this case there is no segregation, and in fact, through a positive correlation in the concentration fluctuations of NO and ethylene, the reaction rates can theoretically be enhanced, making ozone production faster than normal in large-grid simulations based on relatively smaller mean concentrations.

These numerical experiments were built around the NOAA/NCAR Electra aircraft observations downwind of the Sweeney facility made on August 28. We will work closely with the NOAA Aeronomy Laboratory (AL) in defining the details of the experiment and will collaborate on the analysis of the LESchem results. We have received the background emissions rate and the point source emission rates and used these in the LESchem runs. The LESchem experiment was defined to closely approximate the Lagrangian Reactive Plume model configuration already

completed by NOAA/AL. The emissions of hydrocarbons and  $\text{NO}_x$  were co-released from a single point.

The model was initialized chemically using trace-gas profiles from a daytime LESchem simulation employing the surface natural NO/isoprene emission scenario and anthropogenic emissions supplied by NOAA/AL.

Figure 1 shows surface ozone for the high hydrocarbon emission scenarios respectively

#### A-6. Conclusions

Preliminary results from idealized plume studies using a coupled LES-photochemical model indicate potential for rapid formation of small pockets of high  $\text{O}_3$  concentrations within a few kilometers of industrial sources. Heterogeneous photochemical scenarios produce intensity of segregation ( $I_s$ ) values that vary significantly in space and time. Immense and complex LES-photochemical modeling results require further analysis with additional advanced software tools to better understand the net effect of including concentration co-variances on overall boundary layer chemistry

#### A-7. Acknowledgements

This work was jointly supported by an EPA STAR Grant on LES to UAH, SOS EPA Cooperative Agreement, Texas Commission on Environment Quality and internal NOAA funds.

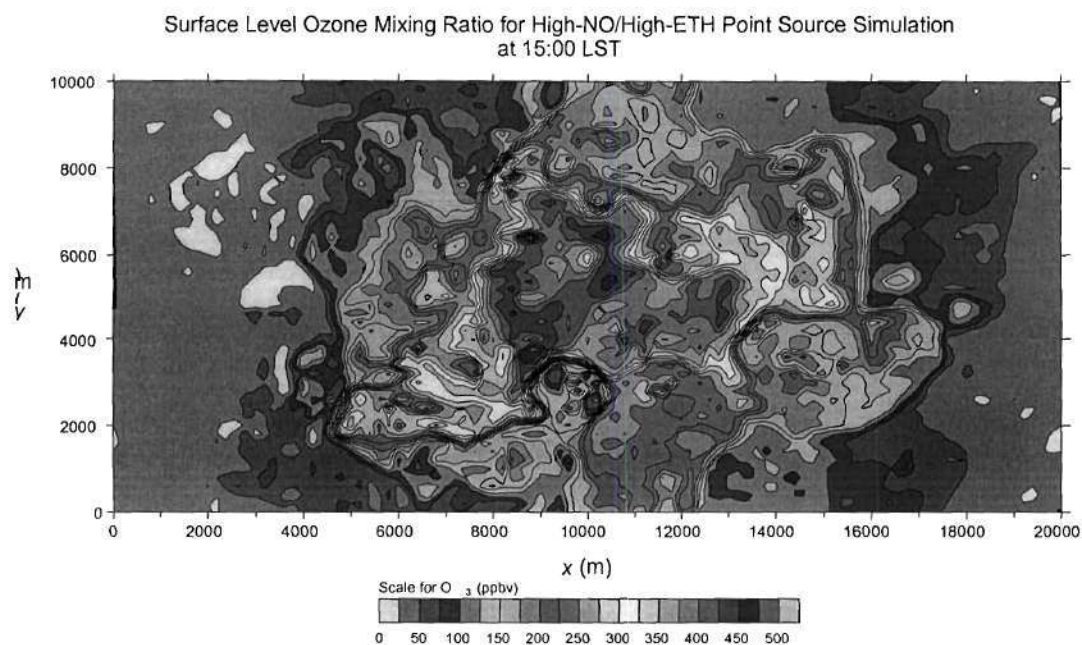


Figure 1. Surface ozone for the aircraft deduced hydrocarbon emissions.

## B. Role of Deformed Flows in Extreme Concentration Events in the Southeast

In air pollution meteorology the conventional wisdom has generally held that the highest pollutant concentrations would occur near the center of a high pressure system. There, light winds and lowered mixing heights (associated with subsidence) would reduce the dilution of surface-emitted pollutants. However, in a study of the regional meteorological conditions associated with high ozone concentrations in the Southeast, it was found that a majority of the extreme events occurred in association with frontal zones or were associated with mesoscale trough lines. The paper (McNider et al 2004) addresses the characterization, modeling, and interpretation of these frontal zones and their role in air quality.

### **B-1 Survey of High Ozone Events**

As part of preliminary studies under the Southern Oxidant Study (SOS), a retrospective study was carried out to determine the characteristics of high ozone events in the Southeast. This was also continued during the observational phase of SOS 1990-1999. The events examined were often the formally designated “design days” for urban areas in the region since these episodes were utilized in the design of regulatory action. Table 1 summarizes ozone levels and episode dates from this survey.

**TABLE 1. Ozone Episodes Occurring in the Southeastern United States Examined**

Period	Maximum 1-hr. avg. concentration (ppb) <sup>1</sup>
July 12, 1983	148
July 25 – August 3, 1987	201
May 31, 1988	158
June 20 – July 1, 1990	187
August 2-3, 1990	141
August 17, 1990	145
August 9-11, 1992	132
July 20-22, 1993	153

<sup>1</sup>Taken from the Aerometric Information Retrieval System of the U. S. Environmental Protection Agency.

### **B-2. Analysis of Deformed Flows and Relation to Stationary Fronts**

The role of stationary fronts and mesoscale trough lines in producing extreme events is not fully clear however it is hypothesized that deformed flows can produce zones of light winds that reduce the dilution of emissions. Hydrodynamic flows can be characterized as made up of four distinct pure flows – pure translation, pure rotation, pure convergence and pure deformation (see figure 2). The combination of pure rotation plus pure deformation gives a flow state that approximates that of a stationary front (see Figure 3).

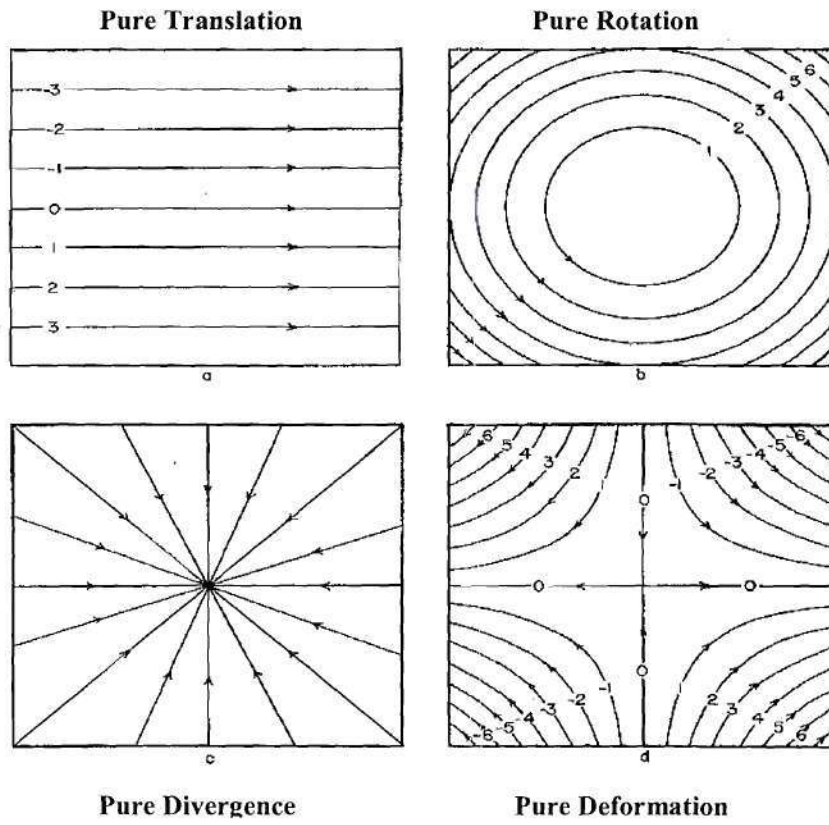


**Figure 2.** Examples of pure hydrodynamic flows

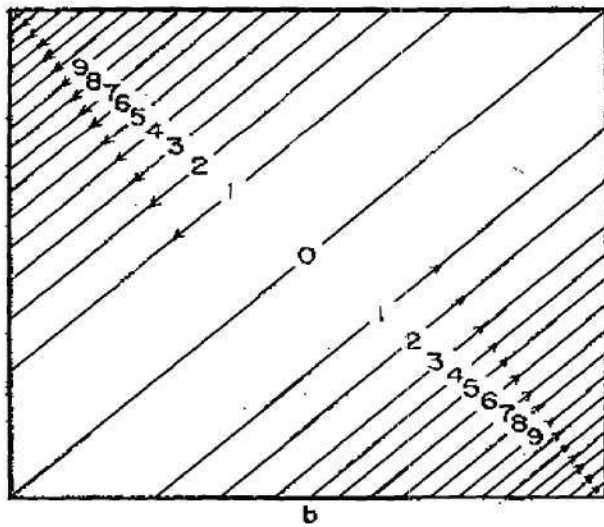


**Figure 3.** Pure deformation plus pure rotation.

An analysis of deformed flows shows that these flows may contribute to conditions of reduced dilution near a front. Consider the advection equation for a pollutant of concentration  $C$

$$\frac{\partial C}{\partial t} + u \frac{\partial C}{\partial x} + v \frac{\partial C}{\partial y} + w \frac{\partial C}{\partial z} = S, \quad (1)$$

where  $S$  represents pollution sources. We apply the equation to an industrial region having an west-to-east extent of  $2L$  and a south-to-north extent of  $2W$ . We superimpose a rectangular Cartesian coordinate system over the region such that the origin is at the region's center as shown in Figure 4.

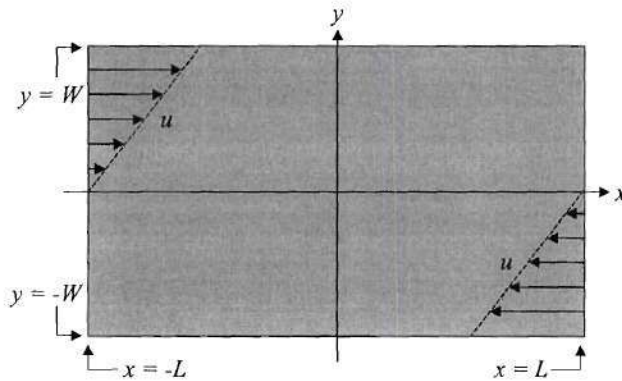


**Figure 4.** An idealized industrial region which is subjected to a deformation flow having a west-to-east stagnation line through the center of the region.

If we assume the wind flow is deformational, having a stagnation line coincident with the  $x$ -axis with westerly winds in the northern half of the region, easterly winds in the southern half of the region, and no vertical motion (again refer to Figure 1), then (1) simplifies to

$$\frac{\partial C}{\partial t} + u \frac{\partial C}{\partial x} = S. \quad (2)$$

We will assume that the magnitude of the flow velocity increases linearly with the increase of distance from the stagnation line and thus may write  $u$  as

$$u = ay, \quad (3)$$

where  $a > 0$  is a constant. To further simplify the problem, we assume that the source term represents a constant surface emission, homogeneous over the region, for a single unreactive

pollutant. If the boundary-layer height is uniformly  $h$  over the region, then we may write  $S$  as

$$S = Q/h, \quad (4)$$

where  $Q$  is the surface pollutant flux. Incorporating (3) and (4) into (2), we obtain

$$\frac{\partial C}{\partial t} + ay \frac{\partial C}{\partial x} = \frac{Q}{h}, \quad (5)$$

The boundary conditions of interest to us are

$$\begin{cases} C(-L, t) = 0, & y > 0 \\ C(L, t) = 0, & y < 0 \end{cases}, \quad (6)$$

for  $t > 0$ , and the initial condition is

$$C(x, 0) = C_0, \quad (7)$$

where  $C_0$  is a uniform initial concentration over the whole region. Condition (7) asserts that the region is initially polluted whereas conditions (6) state that the surrounding areas upwind of the region are clean and remain clean.

First, we consider how the pollutant concentration behaves in the upper half-region ( $y > 0$ ). For our purposes, we note that over time the concentrations reach a steady-state level. To see this, let  $\partial C/\partial t = 0$ . Then (5) reduces to

$$\frac{\partial C}{\partial x} = \frac{Q}{ayh} \quad (8)$$

and has the solution

$$C = \frac{Q}{ayh}(x + L) \quad (9)$$

taking into account the first boundary condition in (6). From (9) we see that eventually the concentration level at a point  $(x, y)$  in the northern half-region reaches the level given by the right side of (9). We further see from (9) that the concentration increases from zero on the western boundary to  $2QL/ayh$  on the eastern boundary and that the concentration decreases as  $y$  increases. A similar analysis can be made for the southern half-region.

Now consider concentration behavior along the stagnation line. Here  $y = 0$ , reducing (5) to

$$\frac{\partial C}{\partial t} = \frac{Q}{h}, \quad (10)$$

which, taking into account the initial condition (7), has the solution

$$C = \frac{Q}{h}t + C_0 \quad (11)$$

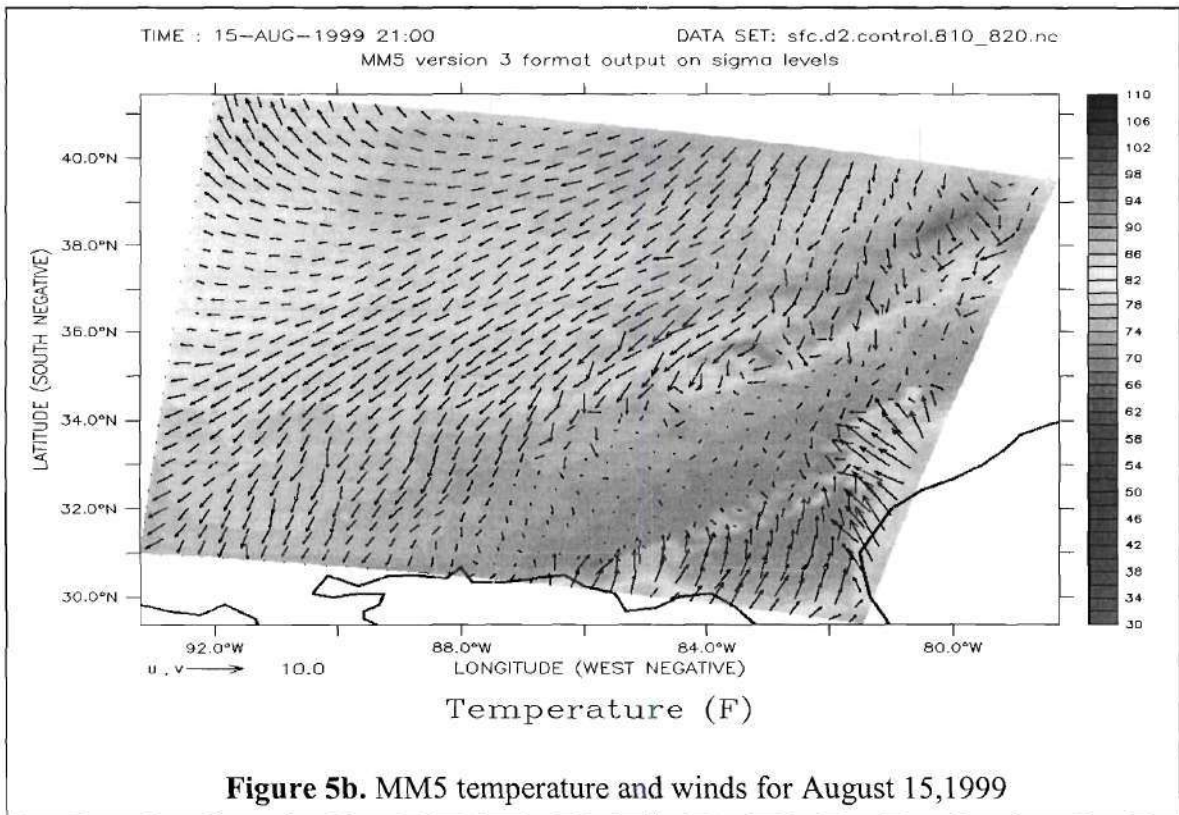
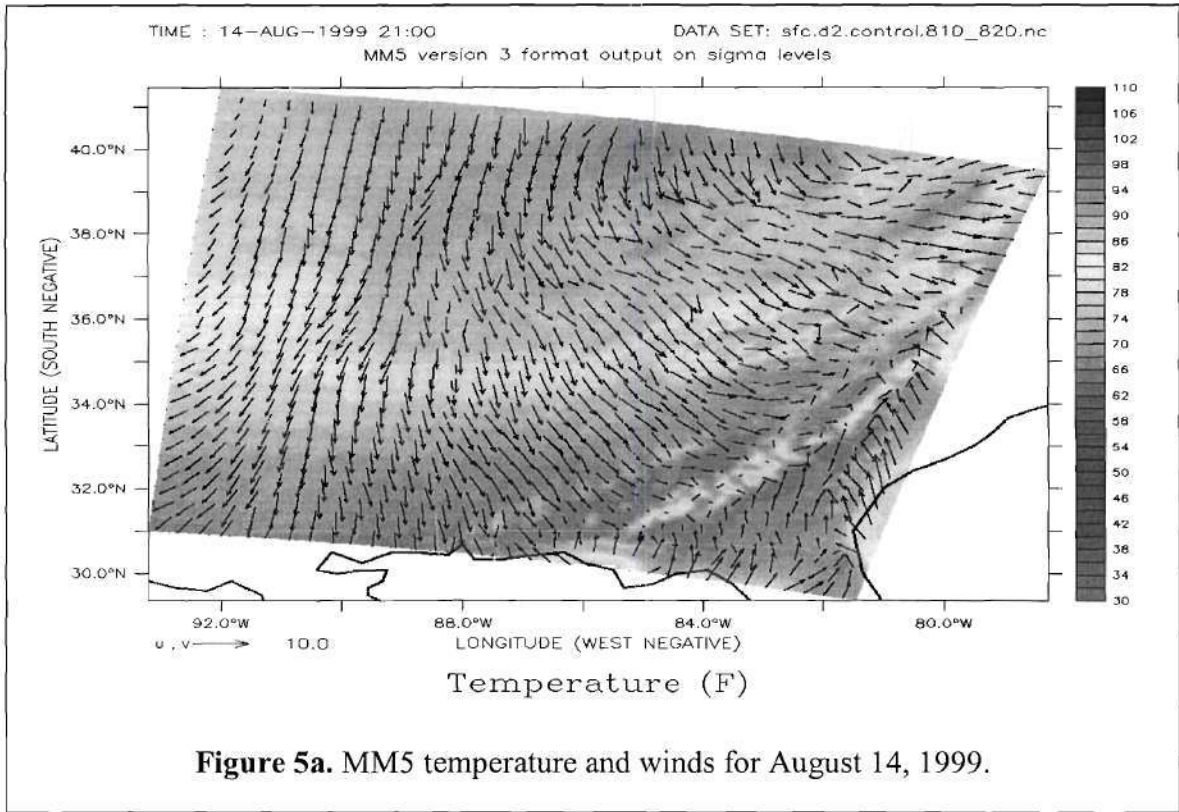
Thus, concentration increases linearly without bound over time along this line. Thus one might expect that the highest concentrations would occur along the stationary front itself.

During simulations made for 1999 with MM5 (see section C below) captured an event that might be indicative of this phenomena. Figure 5a shows wind and temperature plots in a 12 km simulation from MM5 after a weak frontal passage through Georgia. Note northwesterly winds. By the next day (figure 5b) the front has stalled producing a deformed like flow in figure 3. Note the region of calm winds that may contribute to poor dilution and high concentrations.

McNider et al. 2004 provides a complete description and background on the role of deformed flow in producing high concentrations.

### **B-3. Acknowledgements**

This work was supported by the SOS EPA Cooperative Agreement.



### **C. Meteorological Simulations for 1999 SOS Field Intensive Periods**

Beginning in 2000 UAH coordinated with EPA-NERL and TVA in producing a set of meteorological simulations encompassing the Nashville 1999 and Atlanta 1999 intensive observing periods. UAH ran the MM5 model for the period June 16 – August 21, 1999. The model grids and configuration were coordinated with TVA for emissions processing and with EPA for experiments they were conducting over part of the period. As part of an EPA STAR grant UAH was using this period for testing new satellite assimilation techniques. Most of the work during the second and third year has focused on resolving the problems encountered with the satellite assimilation technique for the MM5 simulations for the summer of 1999. The main tasks performed during this period were:

- 1) Verification of early results, comparing the results from MM5 simulations (control and satellite assimilation) with surface observations.
- 2) Formulating a new approach for implementing the assimilation.
- 3) Reprocessing the satellite data to correct for sensor degradation.
- 4) Retrieving cloud information from satellite observations to be used for photochemical modeling.
- 5) Analyzing the role of deformed flows in producing extreme concentration events (see section B).

#### **C-1. Verification of Control and Assimilation Runs of MM5**

A Barnes (1973) analysis scheme fashioned after Koch et al. (1983) was used to create observed analyses of various near-surface variables for the MM5 32-km grid for verification purposes. The observed data for the analysis scheme is the DS472.0 dataset (Technique Development Laboratory (TDL) U.S. and Canada Surface Hourly Observations) obtained from the National Center for Atmospheric Research (NCAR) Data Support Section. This approach gives an observed analysis consistent with spatial distribution of observations, but which is not reliable in data scarce regions such as mountainous terrain where it is a reflection primarily of observations at lower elevations. The observed variables used thus far have been the temperature and water vapor mixing ratio at 2-m. Once the observed analyses have been created, hourly difference fields (model minus the observed analysis) can be calculated and average bias fields constructed.

Figure 6 is an example of average bias fields for temperature at 2-m, respectively, for part of the early portion of the 32-km MM5 simulation for the period 0100 UTC 28 June to 2300 UTC 1 July 1999. In Figure 2 the temperature bias at 2 m for the control run (top) and the satellite

assimilation run (bottom) are displayed. The largest bias values in magnitude are over the Rocky Mountains and the southern Plains. The cool bias values over the Rocky Mountains are the result of the model being cooler than the unreliable surface analyses in those regions because of the lack of representative data. The warm bias of 4°F and above in the southern Plains is evident in both the control and assimilation runs. The satellite assimilation run actually has a larger warm bias than the control run. This was an early attempt using the satellite data assimilation for this case, and later work has discovered the reason for this behavior. Corrections to the satellite data and technique were tested with success for the TEXZQS2000 period (see Han et al. 2004)

The other task related to the 1999 simulations was assistance given to Sun-Kyoung Park (Ph.D. Candidate, Department of Civil and Environmental Engineering, Georgia Institute of Technology (GIT)) in implementing the analysis scheme described above. The analysis scheme is being used to help verify a 13-month long MM5 simulation that is being used as part of a project to refine the emission inventory and establish source-receptor relationships of PM<sub>2.5</sub> in the Atlanta area.

## **C-2. Acknowledgements**

This work was jointly supported by an EPA STAR Grant on Satellite Assimilation to UAH and the SOS EPA Cooperative Agreement.

## **D. Analysis of Winds Observed by Radar Profilers**

As with Nashville 1995 and Nashville 1999, a considerable amount of wind data were collected during TexAQS 2000 to assist in understanding the important features of the wind fields in the Houston area. Besides instruments for measuring surface data, six radar wind profilers and a Doppler lidar were present to provide high temporal resolution of the wind fields from near the surface up to a few thousand meters above the surface at seven locations in the study area. UAH prepared a report for the Texas Natural Resources Conservation Commission (TNRCC) [now the Texas Commission on Environmental Quality (TCEQ)] that describes an initial analysis of the radar profiler data.

Of greatest immediate and practical importance is the guidance this report provides for those who model the TexAQS 2000 period using data assimilation to nudge the computed wind fields toward those that were observed. By means of structure functions, estimates were made of the radius of applicability of wind variables such as the  $u$ - and  $v$ -components of velocity. This type of information is required input for models employing data assimilation.

The question the structure functions help answer is “If a wind value, say wind speed, observed at point A is incorporated into a model, what is the size of the region around A such that the wind speed at A is a good representation of wind speed throughout the region?” Structure functions provide a way to answer the question since the independent variable is distance from a base location and the square root of the dependent variable is the wind characteristic of interest expressed in its original units. This allows us to pose the question in a more quantitative form. Again using wind speed as an example, we can ask “How far from the base location must one travel in order for the average difference in wind speed, due to horizontal separation from the base, to be 1.0 m/s (or any other selected speed)?” Such a distance can be taken as the radius of a circle centered on the base location. The circle is the region of applicability of the wind value. The larger the radius, the more horizontally homogeneous the field of the specified variable.

The magnitude of the radius for a specified amount of change in a wind variable depends on the wind variable chosen. The radius computed for wind speed for a given location will, in general, not be the same as the radius computed for the  $u$ - or  $v$ -component. Each variable has its individual degree of degradation with distance from the base location.

### **D-1. Acknowledgements**

This work was jointly supported by the SOS EPA Cooperative Agreement and the Texas Commission on Environment Quality.

## **E. Development of a Web-Based Lagrangian Particle Model**

The UAH LPM has proved to be a useful tool for visualizing the transport and dispersion of atmospheric emissions. Since the model uses particles only as massless tracers, it is equally applicable to either gaseous or fine particulate emissions. When used in retrospective analyses of field study data, the model can help to determine whether and when plumes passed over monitor sites or whether aircraft flight paths intersected plumes. Based on conditioned particle

concepts (Smith, 1968) in which the Lagrangian turbulent velocity fluctuation of a non-buoyant tracer particle is linearly related to the turbulent fluctuation of the previous time step, the model deduces subgrid-scale velocities (turbulence) from the mean flow parametrically. Unlike simpler models, which use only mean flow to compute a single trajectory, the LPM simultaneously computes the trajectories of many particles. By accounting for the effects of both the mean flow and turbulence on each particle, the model is able to depict both transport and dispersion of plumes.

Time series of mean meteorological fields are provided to the LPM by mesoscale models such as RAMS and MM5. The LPM inherits the domain and grid resolution of the meteorological model (although the data may need to be interpolated from one type of grid structure to another). The user determines where emission points should be located and the rate at which particles are to be released from those points. The sources may be elevated. A plume-rise algorithm is included to handle buoyant emissions. Output consists of a series of snapshots of particle positions within the model domain. One such is duplicated in Figure 10. A time series of such snapshots can be animated.

UAH modified the LPM so that it can be operated through a web-page interface. This involved four main tasks: (1) converting the MM5 file produced by Texas A&M for the TexAQS 2000 study period to suitable input for the LPM, (2) developing a web-page interface for the model, (3) modifying the LPM to make it functional in a web-based environment, and (4) adapting the graphics programs needed to display the LPM results on the web. The interface gives the user the opportunity to tailor a run to fit the specifications of a particular problem. The user selects a domain (108-km, 36-km, or 12 km horizontal resolution), a period of simulation, source locations and types (buoyant or non-buoyant), and the exit conditions (for buoyant sources). When the form containing these choices is completed, the user submits it and waits for the LPM to run. When it is completed, the user is given access to a temporal sequence of particle-position snapshots depicting transport and dispersion of particles released from the sources.

### **E. Development of a Web-Based Lagrangian Particle Model**

The UAH LPM has proved to be a useful tool for visualizing the transport and dispersion of atmospheric emissions. Since the model uses particles only as massless tracers, it is equally applicable to either gaseous or fine particulate emissions. When used in retrospective analyses of field study data, the model can help to determine whether and when plumes passed over monitor sites or whether aircraft flight paths intersected plumes. Based on conditioned particle concepts (Smith, 1968) in which the Lagrangian turbulent velocity fluctuation of a non-buoyant tracer particle is linearly related to the turbulent fluctuation of the previous time step, the model deduces subgrid-scale velocities (turbulence) from the mean flow parametrically. Unlike simpler models, which use only mean flow to compute a single trajectory, the LPM simultaneously computes the trajectories of many particles. By accounting for the effects of both the mean flow and turbulence on each particle, the model is able to depict both transport and dispersion of plumes.

Time series of mean meteorological fields are provided to the LPM by mesoscale models such as RAMS and MM5. The LPM inherits the domain and grid resolution of the meteorological model

(although the data may need to be interpolated from one type of grid structure to another). The user determines where emission points should be located and the rate at which particles are to be released from those points. The sources may be elevated. A plume-rise algorithm is included to handle buoyant emissions. Output consists of a series of snapshots of particle positions within the model domain. One such is duplicated in Figure 10. A time series of such snapshots can be animated.

UAH modified the LPM so that it can be operated through a web-page interface. This involved four main tasks: (1) converting the MM5 file produced by Texas A&M for the TexAQS 2000 study period to suitable input for the LPM, (2) developing a web-page interface for the model, (3) modifying the LPM to make it functional in a web-based environment, and (4) adapting the graphics programs needed to display the LPM results on the web. The interface gives the user the opportunity to tailor a run to fit the specifications of a particular problem. The user selects a domain (108-km, 36-km, or 12 km horizontal resolution), a period of simulation, source locations and types (buoyant or non-buoyant), and the exit conditions (for buoyant sources). When the form containing these choices is completed, the user submits it and waits for the LPM to run. When it is completed, the user is given access to a temporal sequence of particle-position snapshots depicting transport and dispersion of particles released from the sources.

### **3.0 CMAQ Development and Application: Implementation of the Direct Decoupled Method of Computing Sensitivity into CMAQ for Aerosol Species and Application to Understanding Source-Receptor Relationships in the Southeast**

Recently, work has been conducted at Georgia Tech to integrate the Direct Decoupled Method (DDM) for computing sensitivities into the latest release version of the CMAQ model (Cohan et al., 2002, Tian et al., 2004: see attached). This work, however, was focused only on the gas species included in SAPRC99 chemical mechanism. Most of the effort was concentrated on computation of the ozone sensitivities. Realizing the range of useful applications that resulted from this work, it was decided to expand it to include aerosol species of SAPRC99 as well.

Part of the attraction for implementing DDM into CMAQ comes from the fact that the same computational routines in CMAQ that are used to process concentrations can also be adapted to compute sensitivities. This is easier done for linear and well behaved processes. For this reason, a large portion of the discussion about DDM is necessarily about understanding the existing CMAQ code.

Sensitivity analysis is an important tool for policy-makers and scientists to develop control strategies for pollutants. As compared to the traditional Brute Force approach, the Direct Decoupled Method allows for more efficient computation of several responses in a single run (in most cases). Presented here is a summary of this new work and the latest result, as well as current difficulties and issues that require additional attention.

A small test domain was created centered over the State of Georgia for which the results are presented. The code was also tested on a 36-km resolution domain used in the Fall Line Air Quality Study (FAQS) that represents the eastern half of the US as well as an ASACA project domain that includes the entire country. DDM sensitivities are compared to those computed by Brute Force in order to assess the validity of this method. Both types of sensitivities are computed to the emissions of NO<sub>x</sub>, SO<sub>2</sub>, NH<sub>4</sub>, biogenic organics, and anthropogenic organics.

#### **3.1 CMAQ Aerosol Species of Interest**

A list of aerosol species used in the SAPRC99 chemistry mechanism is attached as Appendix A. Aerosol species are split into three modes – Aitken, Accumulation, and Coarse. Aitken mode represents fresh particles from both nucleation and direct emission, while the Accumulation mode represents the bigger aged particles. These two modes interact through coagulation, and each experiences other aerosol processes such as deposition, condensation of gases, emissions, etc.

Inorganic chemicals tracked by CMAQ include sulfate, nitrate, and ammonium. The organics are split into biogenic, anthropogenic, as well as primary anthropogenic. All of these species exist in both the Aitken and Accumulation mode. Coarse mode species include sea salt and wind-blown dust.

At this time, DDM has been implemented for sulfate, nitrate, ammonium, biogenic organics, and anthropogenic organics.

#### **3.2 CMAQ routines important for aerosols**

As mentioned above, much of the work for integrating DDM into CMAQ has already been completed. Processes such as advection, diffusion, chemistry of gas species important to aerosol production are already capable of handling computations of aerosol DDM. What remained were the processes important primarily for changing aerosol concentrations. These processes are discussed below and are grouped into two broad categories of aqueous chemistry and aerosol interactions.

### 3.3 Aqueous Chemistry

CMAQ recognizes a presence of a cloud in a given cell when the relative humidity in that cell is sufficient to activate aerosol particles and turn them into cloud droplets. These droplets provide the means of removal of concentrations by rain-out and scavenging. Furthermore, these droplets provide the media for aqueous-phase chemical equilibria and reactions.

#### 3.3.1 Scavenging and Wet Deposition

Scavenging and Wet Deposition are a simple linear process in CMAQ. It can be summarized by the following formula for any given cell:  $C_f = C_i * e^{(-\alpha\tau)}$ , where  $\tau$  is the length of the time step and  $\alpha$  is a scavenging coefficient.

It was assumed that sensitivities would follow the same model ( $S_f = S_i * e^{(-\alpha\tau)}$ ), using the same scavenging coefficient. The scavenging coefficient is never a function of any sensitivity parameter, making this a valid method.

#### 3.3.2 Oxidation of SO<sub>2</sub>

Oxidation of SO<sub>2</sub> and subsequent conversion to sulfate aerosol follows five pathways in CMAQ. Sulfur can be oxidized by hydrogen peroxide, ozone, metals (Fe<sup>+++</sup> and Mn<sup>++</sup>), methyl hydrogen peroxide (MHP), and peroxyacetic acid (PAA). The rates of conversion through the majority of these pathways are calculated based on empirical data. They are presented as rate expressions for different ranges of pH and amount of sulfur available.

Since conceptually, sensitivity is a derivative, it was computed as such for each of the rate expressions. For example, at pH that is not very low (above 2.7), the oxidation rate due to ozone is expressed as follows:

$$DSIVDT(O3) = -4.19E5 * (1.0 + 2.39E-4 / AC) * O3L * SIV$$

Here, AC is the concentration of H<sup>+</sup>, O3L is the dissolved ozone, and SIV is dissolved SO<sub>2</sub>. The rate of change of sensitivity thus becomes:

$$S\_DSIVDT(O3) = -4.19E5 * (1.0 + 2.39E-4 / AC) * (S\_O3L * SIV + S\_SIV * O3L) - 2.39E-4 * AC^{**(-2.0)} * S\_AC * O3L * SIV$$

In this expression, the S<sub>\_</sub> denotes the sensitivity of the species as opposed to concentration.

The pH is calculated using the method of reiterative bisection through a charge balance of all ions. However, it is not possible to approximate the sensitivity of pH to a given parameter by the same method. Since the sensitivity of the hydrogen ion is important in accurately calculating certain aerosol sensitivities, it was approximated instead by a balance of the sulfate and ammonium sensitivities.

The rates at which concentrations are converted are also used to determine a time sub-step on which all aqueous chemistry calculations are performed. This is based on the minimum amount of time required to convert a set amount of sulfur through any one of the five pathways. It is assumed that sensitivities follow the same timescale as concentrations.

### 3.3.3 Below-cloud Diffusion

CMAQ clouds are divided into two categories – resolved and unresolved. Resolved clouds occupy the entire grid cell. Thus, the effects of aqueous chemistry on concentrations and sensitivities concern the entire cell. Unresolved clouds fill the grid cell only partly. The effects of aqueous chemistry in these clouds are “diluted” by the air outside the cloud. Furthermore, there is a cloud driven movement and mixing of gases and aerosols in the column below the cloud.

At this time, it assumed that sensitivities follow exactly the routines defined for concentrations in regard to mixing below the cloud as well as mixing with air outside. However, there is evidence that this is not always a good assumption and that developing a special way to treat below-cloud diffusion for sensitivities might improve final results.

## 3.4 Aerosol Interactions

### 3.4.1 Inorganic Aerosols

The main concern in the aerosol subroutines of CMAQ for DDM sensitivity computation revolves around aerosol/gas equilibrium for each of the inorganic groups as well as a charge balance for all species. DDM has been implemented for aerosol before at Georgia Tech for the URM model by Boylan et al. (2002). While the species available in URM and the species in the SAPRC99 mechanism are slightly different, it was possible to adapt some of their work for CMAQ.

Both URM and the latest version of CMAQ use the ISORROPIA model which computes the state and the speciation of inorganic aerosol (Nenes et al., 1998). Boylan et al. created a matrix for the unknown sensitivities of all species in ISORROPIA by taking the derivative of each equilibrium expression.

For example, the reaction  $\text{HSO}_4^-(\text{aq}) \xrightleftharpoons{k_f} \text{H}^+(\text{aq}) + \text{SO}_4^{2-}(\text{aq})$  leads to a rate expression (ignoring activity coefficients)  $[\text{SO}_4^{2-}] = k_f [\text{HSO}_4^-]/[\text{H}^+]$ . Taking the derivative would result in:

$$\delta[\text{SO}_4^{2-}]/\delta P_i = -([\text{SO}_4^{2-}]/[\text{H}^+]) (\delta[\text{H}^+]/\delta P_i) + ([\text{SO}_4^{2-}]/[\text{HSO}_4^-]) (\delta[\text{HSO}_4^-]/\delta P_i)$$

Here,  $P_i$  is any sensitivity parameter of interest.

Such expressions were calculated for each equilibrium reaction of all inorganic species as well as mass conservation expressions and charge balances. The resulting matrix is also capable

of computing sensitivities of species that are not tracked CMAQ at this time, such as species involving sodium and chlorine. These species are ignored currently for sensitivities, but are ready for use in the future if they are introduced in CMAQ.

One of the more recent additions to CMAQ has been a change to the treatment of the  $N_2O_5 / HNO_3$  system. This has some effect on the aerosol sensitivities because it is sometimes a removal of  $HNO_3$  effecting the sensitivities of nitrate. Currently, it is assumed that the rate of *conversion of sensitivity* is the same as that for concentration.

### 3.4.2 Organic Aerosols

Computation of the organic aerosol sensitivities parallels the subroutines that partition the semi-volatile species concentrations. A list of these species is found in Appendix B. CMAQ establishes equilibrium of these species and then calculates the gas and aerosol phase concentration of each species iteratively. The species are then summed into the appropriate category – organic or inorganic.

It is not possible to calculate the sensitivities in the same way as concentrations, because the iterative method relies on finding roots and does not behave well with negative numbers that are possible with sensitivities. Instead, it was assumed that it is possible to calculate a partitioning coefficient  $K$ , such that  $K_i = C_{i(\text{aerosol})} / C_{i(\text{gas})}$ . This is a good first order approximation of the way that concentrations are behaved each time-step. This partitioning fraction was then applied to compute how much of the volatile gas sensitivity would go into aerosol phase.

### 3.5 Results

The results are presented as a comparison between Brute Force sensitivities and those computed by the Direct Decoupled Method. Shown here is the 36-km resolution domain used in the Fall Line Air Quality study at Georgia Tech. Each figure shows the response to 100% increase in emissions of a certain pollutant. Brute Force was computed by taking the difference of the results of the 110% emissions run and the 90% emissions run and multiplying it by 5 to approximate the sensitivity in the same range as DDM. These simulations were run for a two day period of August 11 and 12, 2000. All of the results are shown for the accumulation mode where majority of the mass is found. Also, the time-series plots show a domain-wide average and are intended to demonstrate temporal agreement between the two methods.

### 3.5.1 Sensitivity to SO<sub>2</sub> Emissions.

The first set is the comparison of sulfate sensitivity to emissions of SO<sub>2</sub> domain wide.

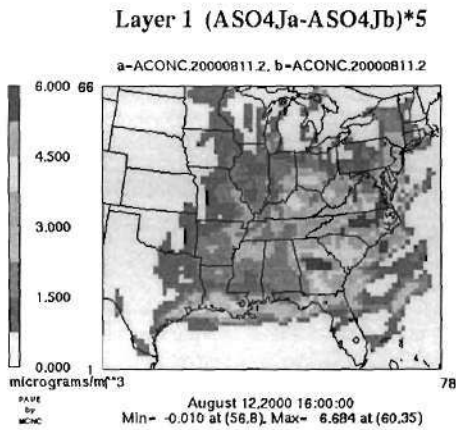


Figure 6a. Brute Force SO4

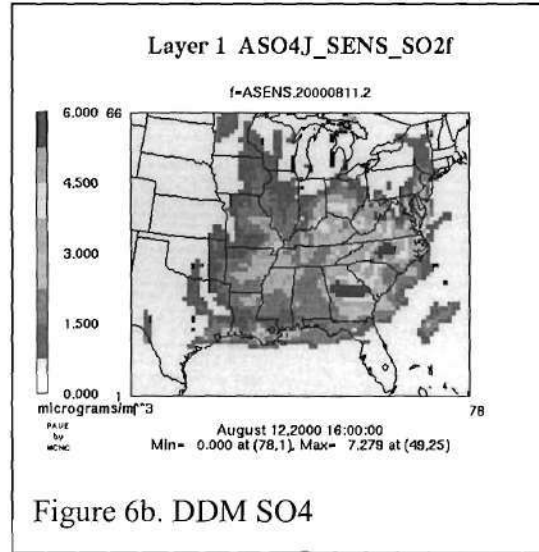


Figure 6b. DDM SO4

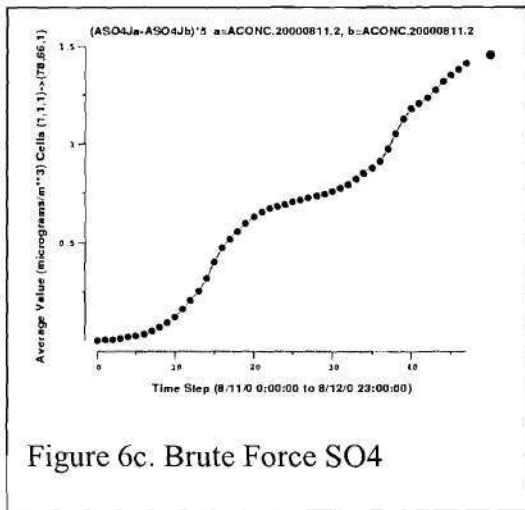


Figure 6c. Brute Force SO4

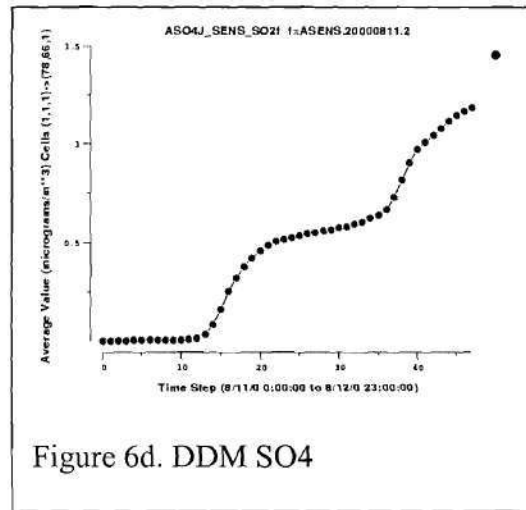


Figure 6d. DDM SO4

Sulfate DDM sensitivity behaves in a very similar way to that shown by BF. It requires a little bit of a “ramp-up” period as evident by the time-series plot in Fig. 6d. Areas where DDM deviates most significantly from BF are along the coast that had a significant cloud-cover during this period. This indicates that more work needs to be done on the aqueous chemistry routines to improve performance there.

### 3.5.2 Sensitivity to NOx emissions.

The second set of figures shows the results for the domain-wide NOx emissions. The results are for the sensitivity of nitrate.

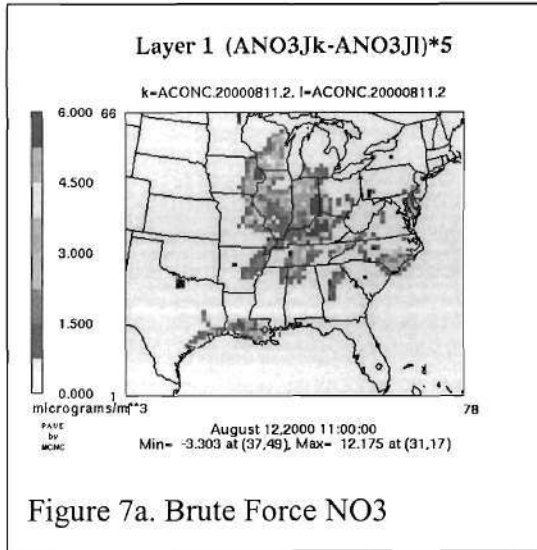


Figure 7a. Brute Force NO3

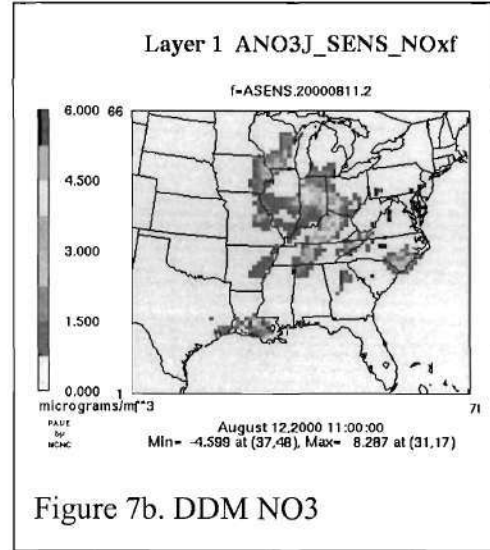


Figure 7b. DDM NO3

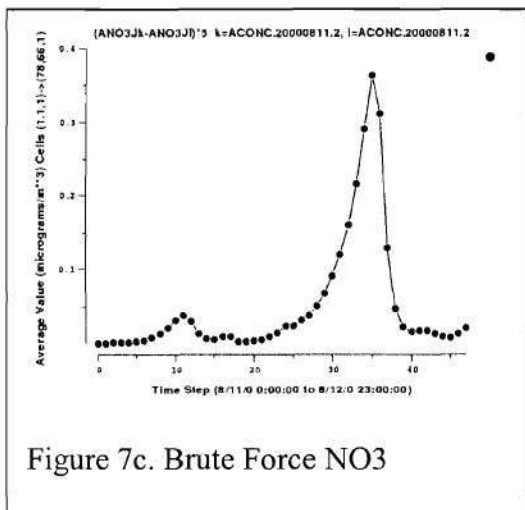


Figure 7c. Brute Force NO3

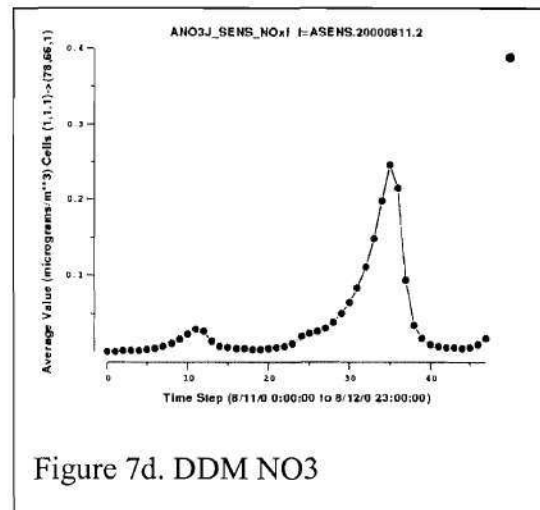
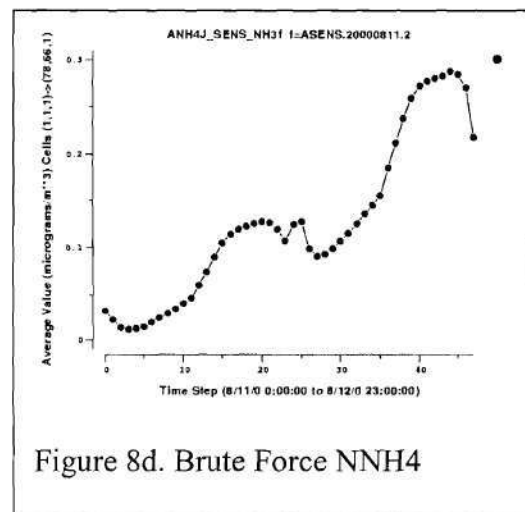
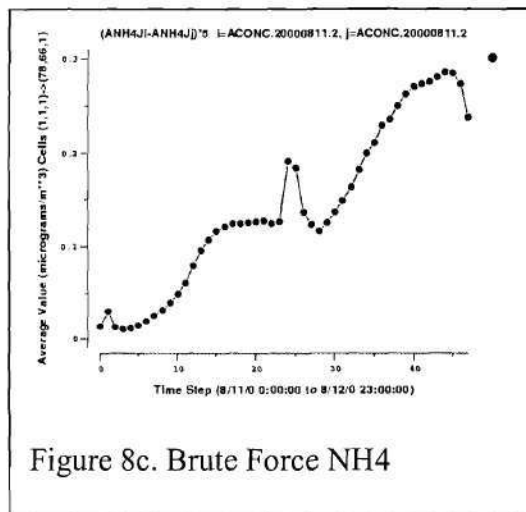
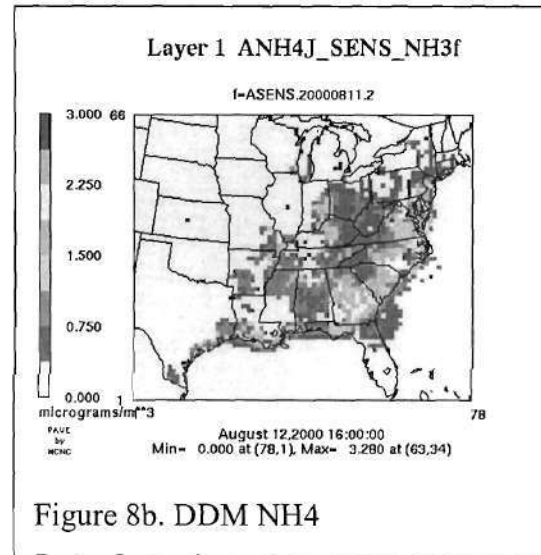
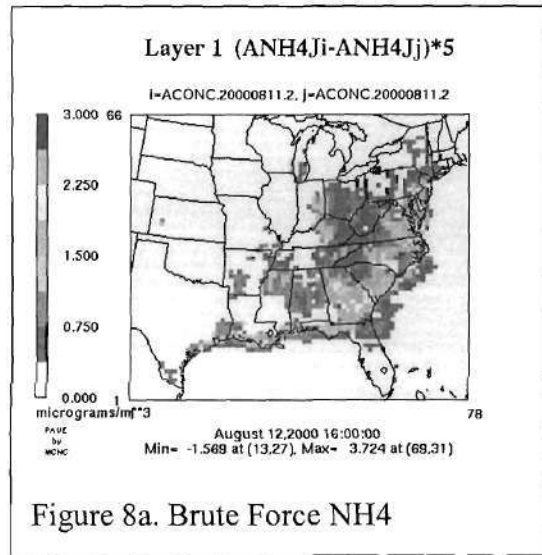


Figure 7d. DDM NO3

It is evident that while the special distribution of the DDM sensitivity matches very well with the BF, there is a slight under-estimation.

### 3.5.3 Sensitivity to NH<sub>3</sub> emissions.

While ammonium is classified as one of the non-reactive species and does not participate in gas phase chemistry in CMAQ, it has a significant impact on aerosol concentrations through ISORROPIA. Shown here are the results for the sensitivity of the ammonium aerosol to domain-wide NH<sub>3</sub> emissions.



The sensitivity of ammonium aerosol shows a good comparison despite a tendency of both BF and DDM to show some unusual spikes.

### 3.5.4 Sensitivity to Xylene emissions.

Xylene was used as a surrogate to represent total anthropogenic emissions. The computations for xylene sensitivities are exactly the same as those for other anthropogenic, so getting good agreement here would indicate the rest are performing well. Shown here are, again, are sensitivities of anthropogenic organic aerosol to domain-wide emissions of xylene.

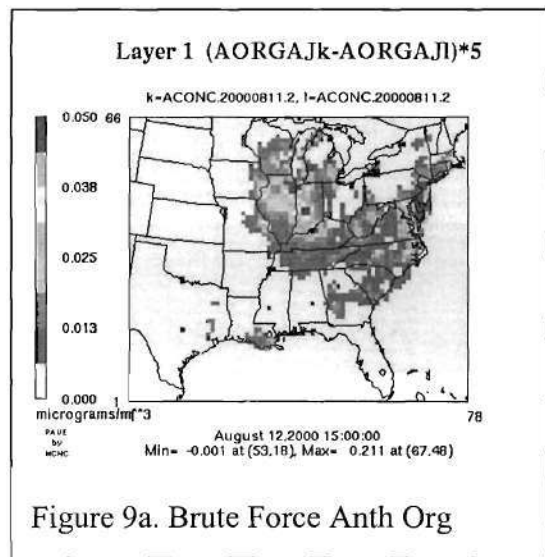


Figure 9a. Brute Force Anth Org

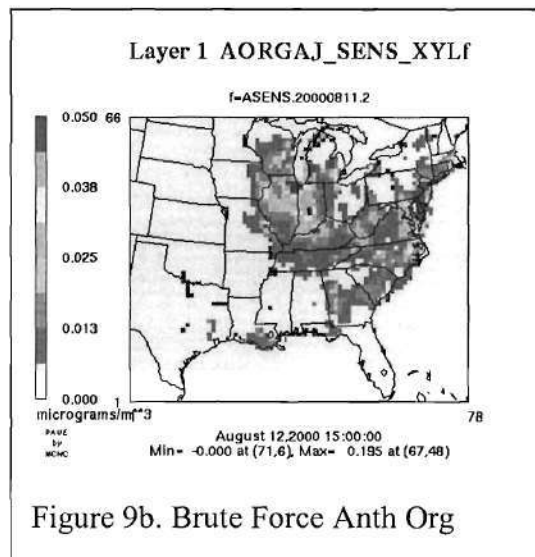


Figure 9b. Brute Force Anth Org

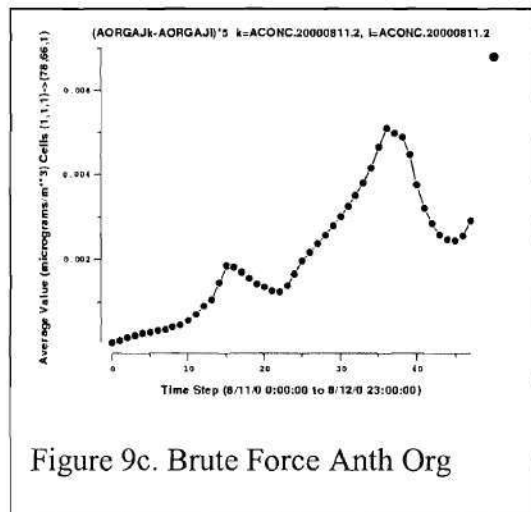


Figure 9c. Brute Force Anth Org

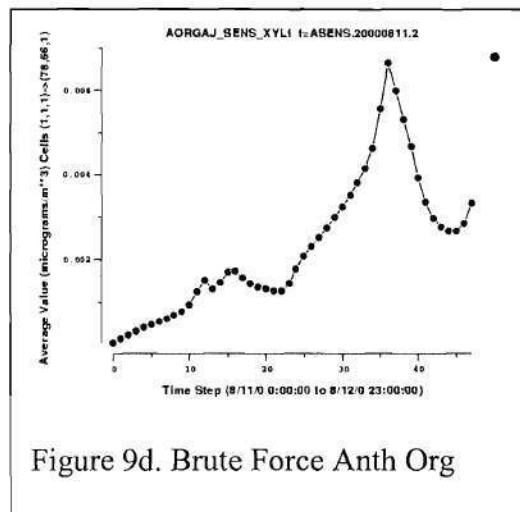


Figure 9d. Brute Force Anth Org

This shows a very good agreement and only a slight overestimation in the time-series plot.

### 3.5.5 Sensitivity to Terpene emissions.

Again, only one representative compound was chosen for biogenic emissions. In the following graphs, the sensitivities of biogenic organics are shown to domain-wide emissions of terpene.

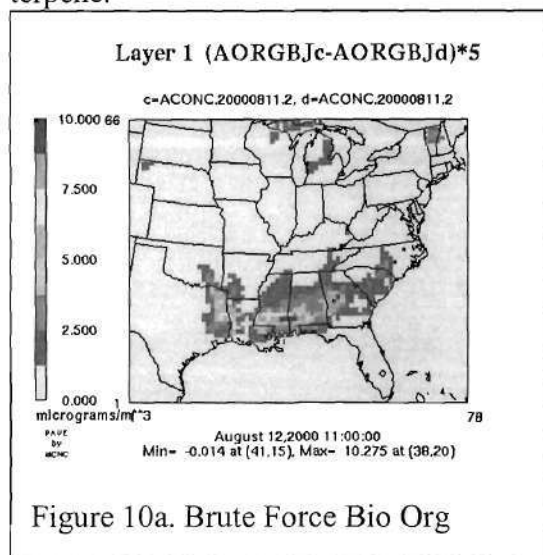


Figure 10a. Brute Force Bio Org

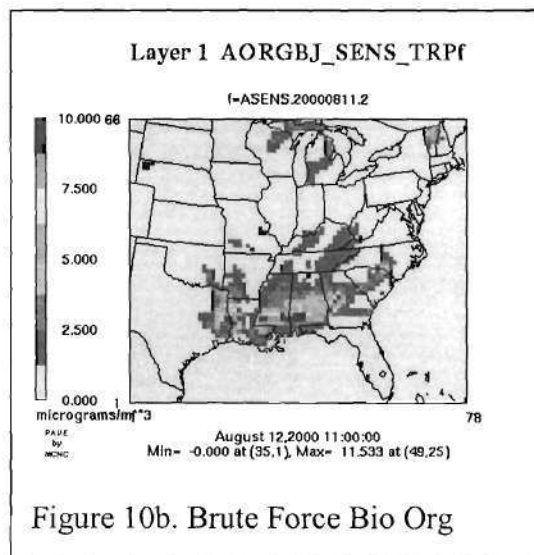


Figure 10b. Brute Force Bio Org

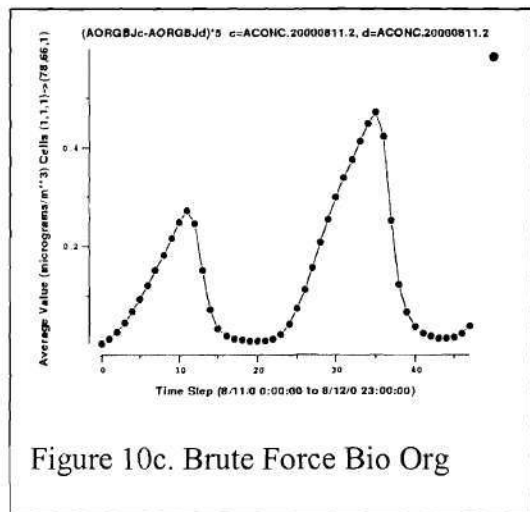


Figure 10c. Brute Force Bio Org

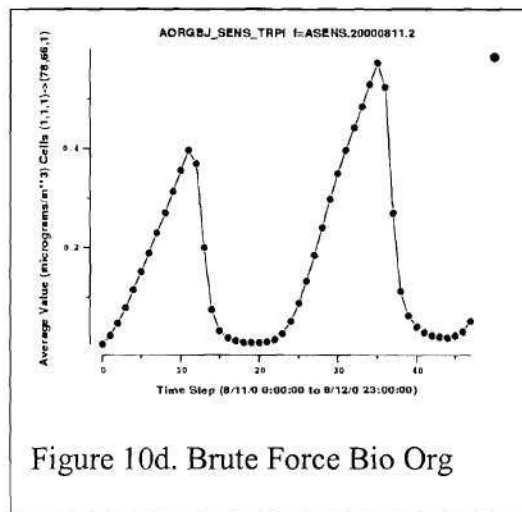
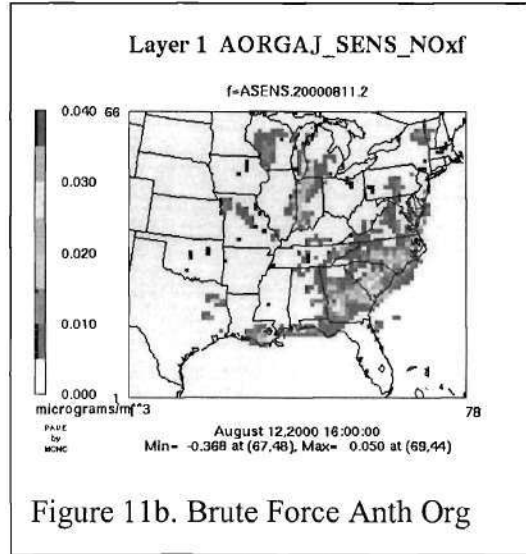
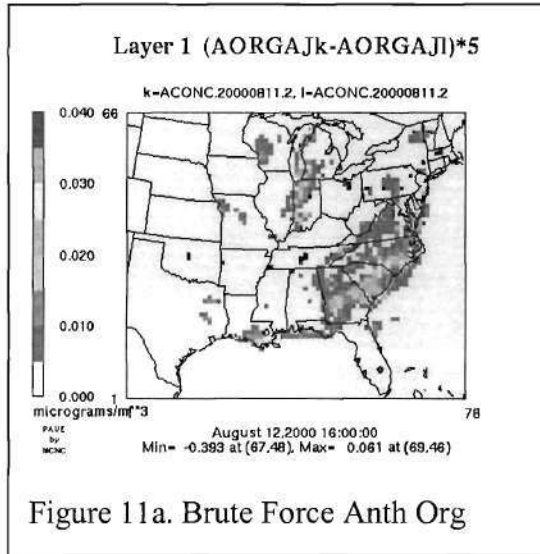


Figure 10d. Brute Force Bio Org

The results are similar to those of anthropogenics. There is fairly good special distribution with a slight overestimation in the case of DDM.

### 3.5.6 “Cross-specie” sensitivities

All of the results above were show as species sensitive to their “parent” gases. For example, sulfate aerosol is created from oxidation of SO<sub>2</sub>, so the sensitivity of sulfate was shown to the emissions of the gas. However, sensitivities of species not directly related are also interesting and important. These are harder to approximate with DDM, but many still show good agreement. For example, here is spatial plot comparison for the sensitivity of anthropogenic organic aerosol to domain-wide emissions of NO<sub>x</sub>.



A full table of different possibilities of sensitivities is shown below.

TABLE 2. Summary of Results

	<b>Sensitivities to the Emissions of :</b>				
<b>Species:</b>	<b>SO2</b>	<b>NOx</b>	<b>NH3</b>	<b>Xylene</b>	<b>Terpene</b>
<b>Sulfate</b>	Fair	Fair	Poor	Small	Fair
<b>Nitrate</b>	Poor	Good	Good	Fair	Fair
<b>Ammonium</b>	Fair	Good	Good	Fair	Fair
<b>Anth. Org.</b>	Small	Good	Small	Good	Small
<b>Bio. Org.</b>	Small	Fair	Small	Small	Good

### 3.6 Conclusions

The Direct Decouple Method was integrated into the current CMAQ code successfully for the majority of the aerosol species. There are some performance issues in some sensitivities that are not “matched-pairs.” For example, the sensitivity of nitrate to SO<sub>2</sub> needs improvement.

Furthermore, some processes can be improved on to increase both efficiency of computation and also accuracy of DDM. The way below-cloud diffusion is handled would be an example of this situation. There are some issues involved in mass conservation in the original CMAQ code, and ISORROPIA has some strange sensitivity responses that need to be addressed. Gas phase application, as conducted with funding from both this project, and much more so from FAQS, showed the power of DDM for conducting source apportionment and sensitivity studies.

#### **4.0 NARSTO archiving of the 1999 Atlanta Supersite data**

##### **THE ATLANTA SUPERSITE**

The 1999 Atlanta Supersites Project was conducted during August 1999 in Atlanta, Georgia. This 4-week intensive study (August 3 to September 1, 1999) brought together over 150 scientists and technicians making a variety of measurements using advanced state-of-the-science systems, such as the particle mass spectrometers, semi-continuous species specific PM methods, and discrete chemical speciation samplers for mass and the major chemical components of mass.

The study was coordinated by the Southern Oxidants Study (SOS) in collaboration with numerous universities and agencies that comprise SOS as well as several on-going air quality research programs occurring in Atlanta at the time of this study. The Atlanta Supersites Project was located at the existing SEARCH/ARIES site on Jefferson St. in NW Atlanta, GA.

The primary objective of the Atlanta Supersites Project was to evaluate and compare advanced measurement methods for particulate matter mass and its components. Methods included filter/denuder based time-integrated or discrete samplers, a variety of semi-continuous methods measuring mass, its major components (sulfate, nitrate, ammonium, organic carbon, elemental carbon, trace elements) and gas phase precursors, and for the first time ever, a comparison among particle mass spectrometers, four in total.

These data were complemented by meteorological data as well as gas phase criteria pollutant measurements and other supplemental data, such as particle physical properties, VOC, oxygenated VOC, and NO<sub>y</sub>. The primary and supplemental data also were used to better understand the formation and accumulation of PM in Atlanta and to better understand source-receptor relationships.

##### **THE ATLANTA DATABASE**

The comprehensive database developed as a result of this study is available to the general public through the NARSTO web site. This long-term archival and public distribution of NARSTO validated electronic data and data products is located at the NARSTO Permanent Data Archive (PDA) operated by the NASA Langley Research Center Distributed Active Archive Center (DAAC). The Langley DAAC provides no-cost ordering and FTP retrieval of NARSTO project data at [URL: http://eosweb.larc.nasa.gov/PRODOCS/narsto/table\\_narsto.html](http://eosweb.larc.nasa.gov/PRODOCS/narsto/table_narsto.html) Information about the archiving process is available at the NARSTO Quality System Science Center (QSSC) at [URL: http://cdiac.esd.ornl.gov/programs/NARSTO/narsto.html](http://cdiac.esd.ornl.gov/programs/NARSTO/narsto.html). Atlanta Supersites project data files are stored in the NARSTO Data Exchange Standard (DES) format. Data Exchange Standard files are self-documenting, with the essential information contained in the same file as the data.

These files are easily read by spreadsheets and relatively easy to create with spreadsheets software. They are saved as ASCII comma-separated value (.csv) files. Data Exchange Standard files are composed of key phrases, metadata tables and data tables. Metadata is information about the content, quality, condition and additional characteristics of the data. Typical metadata tables includes a station information table, a measurement method information table, a lookup table where codes appearing in data tables are cross-referenced with descriptions, and a measurement data table that contains the actual data. The measurement data table besides presenting the actual data, it provides information about the when

and where of the collection of measurement of each value, define any missing value, and provides references to definitions of standard and/or nonstandard flags as well as any project specific quality codes.

Therefore, A DES file contains header information about the contents of the file and the data originator, metadata entries that identify sites, flags, units, and sampling and analysis methods, and a main data table of measurement results. Appendix A describes a template with the header information records. The DES file can be directly imported into an Excel spreadsheet or other software. Project documentation about the data collection is associated with the data set in the PDA.

When the DES file has been filled in with metadata and data, a copy is saved in ASCII CSV (comma-separated values) format. The ASCII file is the final storage format for the archive. The ASCII file is submitted to the Quality Assurance Center (QAC), currently it is part of the NARSTO QSSC, where the file is run through a set of quality assurance tests. The QAC provides the results of the QA tests (and sometimes statistical summaries and time series plots) to the data originator. The data originator reviews the reports, makes corrections as needed, and resubmits the file to the QAC. After a final check, the ASCII file becomes the master copy of the data and are placed in the archive.

The Atlanta Supersite database comprises 40 files, involving 1,593,549 measurements and submitted to the QAC for QA/QC. All of these 40 files have been accepted for permanent storage at the NARSTO archive. A brief description of these files follows:

#### **FILE NAMING SYNTAX**

All 40 files are identified by the prefix EPA\_SS\_ATLANTA. This is followed by a condensed identifier that briefly describes something about the file (see below for an explanation of the condensed identifiers). Next is the descriptor that identifies if the measurements are particles (PART\_DATA), gases (GAS\_DATA), meteorology (MET\_DATA), a combination (PART\_GAS\_DATA), or profiler data (PROFILER\_DATA). The number that follows separates files of the same type. The syntax ends with the initials of the principal investigator that was responsible for collecting the data. A list of the principal investigators and the associated initials follows: BT: Barbara Turpin; DM: Dick McNider; DS: Dennis Savoie; EE: Eric Edgerton; GA: George Allen; KB: Karsten Baumann; HM: Hal Maring; MB; Michael Bergin; PJ: Piet Jongejan; PM: Peter McMurry; PS: Paul Solomon; RT: Roger Tanner; RW: Rodney Weber; RZ: Rod Zika; SD: Sandy Dasgupta; SH: Susanne Hering; and TR: Ted Russell.

#### **FILE DESCRIPTION**

A description of the 40 files that includes principal investigator, initials identification, principal investigator's affiliation, status, instrumentation used and type of measurements, and condensed identifier, follows:

Barbara Turpin (BT)

Rutgers University

One file accepted for permanent storage

EPA\_SS\_ATLANTA\_ITOPC\_PART\_DATA\_1\_BT\_V1.csv

- In-situ carbon analyzer for semi-volatile, organic, elemental and total carbon
- Condensed identifier - ITOPC : In-situ thermal-optical particulate carbon

Dick McNider (DM)

University of Alabama at Huntsville

Two files accepted for permanent storage

EPA\_SS\_ATLANTA\_UAH-MIPS\_PROFILER\_DATA\_1\_DM\_V1.csv

EPA\_SS\_ATLANTA\_UAH-MIPS\_PROFILER\_DATA\_2\_DM\_V1.csv

- Temperature and wind speed measured at different height by the UAH Mobile Integrated Profiling System
- Condensed identifier - UAH-MIPS : University of Alabama at Huntsville Mobile Integrated Profiling System.

Dennis Savioe (DS)

University of Miami

Three files accepted for permanent storage

EPA\_SS\_ATLANTA\_ANIONS\_MOUDI\_PART\_DATA\_1\_DS\_V1.csv

- MOUDI for ions and trace elements
  - Condenser identifier - ANIONS\_MOUDI : Anions MOUDI
- EPA\_SS\_ATLANTA\_MASS\_MOUDI\_PART\_DATA\_2\_DS\_V1.csv

- MOUDI for mass, heavy molecular weight organic compounds
  - Condenser identifier - MASS\_MOUDI : Mass particles MOUDI
- EPA\_SS\_ATLANTA\_OCEC\_MOUDI\_PART\_DATA\_3\_DS\_V1.csv

- MOUDI for OC,EC
- Condenser identifier - OCEC\_MOUDI : Organic and Elemental Carbon MOUDI

Eric Edgerton (EE)

Atmospheric Research and Analysis, Inc.

One file accepted for permanent storage

EPA\_SS\_ATLANTA\_3-SFDS\_PART\_DATA\_1\_EE\_V1.csv

- PCM particle composition monitor for PM2.5 mass, trace elements, water-soluble metals, ions, organic and elemental carbon. Automated catalytic reduction system for ammonium, nitrate, and sulfate. Commercial R&P for organic and elemental carbon.
- Measurements include sulfate, ammonium ion, nitrate, silicon, potassium, calcium, titanium, manganese, iron, copper, zinc, bromide, and lead.
- Condensed identifier - 3-SFDS : Data from a 3-stage filter-denuder sampler

Petros Koutrakis and George Allen (GA)

Harvard School of Public Health

Three files accepted for permanent storage

EPA\_SS\_ATLANTA\_BC\_EC\_PART\_DATA\_1\_GA\_V1.csv

- Aethalometer measurements of urban elemental carbon and classic black carbon soot
- Condensed identifier - BC\_EC : HSPH Aethalometer urban EC and classic Black Carbon Soot

EPA\_SS\_ATLANTA\_CAMM\_PART\_DATA\_2\_GA\_V1.csv

- Pressure drop mass measurement for PM2.5
- Condensed identifier - CAMM : Continuous Ambient Mass Monitor

EPA\_SS\_ATLANTA\_HSPH\_NO3\_PART\_DATA\_3\_GA\_V1.csv

- Continuous measurements of nitrate NO<sub>3</sub>
- Condensed identifier - HSPH\_NO3 : HSPH Continuous Nitrate Monitor

Karsten Baumann (KB)

Georgia Institute of Technology

Three files accepted for permanent storage

EPA\_SS\_ATLANTA\_PCM\_PART\_GAS\_DATA\_1\_KB\_V1.csv

- PCM: Multi-channel denuder filter pack system for PM2.5 mass, ions, organic carbon (OC), elemental carbon (EC), and gaseous ammonia, nitric and light organic acids, and sulfur dioxide.
- Condensed identifier - PCM : Particle composition monitor

EPA\_SS\_ATLANTA\_MET\_MET\_DATA\_1\_KB\_V1.csv

- Meteorological data: atmospheric pressure, ambient temperature, relative humidity, wind speed and wind direction, global and UV radiation
- Condensed identifier - MET : Meteorological data

EPA\_SS\_ATLANTA\_GAS\_GAS\_DATA\_1\_KB\_V1.csv

- Criteria gases: NO, NO<sub>y</sub>, O<sub>3</sub>, CO, SO<sub>2</sub>
- Condensed identifier - GAS : Gaseous chemical data

Hal Maring (HM)

University of Miami

One file accepted for permanent storage

EPA\_SS\_ATLANTA\_LIGHT\_SCAT\_PART\_DATA\_1\_HM\_V1.csv

- TSI nephelometer for particle light scattering at three wavelengths
- Condensed identifier: - LIGHT\_SCAT : Aerosol light scattering

Michael Bergin (MB)

Georgia Institute of Technology

Two files accepted for permanent storage

EPA\_SS\_ATLANTA\_UV\_BREWER\_MET\_DATA\_1\_MB\_V1.csv

- Ultraviolet downwelling radiation measurements
- Condensed identifier - UV\_BREWER : Ultra-violet radiation measurements

EPA\_SS\_ATLANTA\_PM\_ASAC\_PART\_DATA\_1\_MB\_V1.csv

- PM2.5 mass by relative humidity controlled TEOM and aerosol scattering and absorption coefficients by a spectral radiometer.
- Condensed identifier - PM\_ASAC : PM2.5, Aerosol Scattering & Absorption Coefficient

Piet Jongejan and J. Slanina (PJ)

Netherlands Energy Research Foundation

Two files accepted for permanent storage

EPA\_SS\_ATLANTA\_AWD\_SJAC\_IC\_PART\_GAS\_DATA\_1\_PJ\_V1.csv

EPA\_SS\_ATLANTA\_AWD\_SJAC\_IC\_PART\_GAS\_DATA\_2\_PJ\_V1.csv

- SJAC: Steam jet aerosol collector for chloride, nitrate, sulfate and ammonium ion and automated IC for on-line analysis.
- Rotating wet denuder for collection of HCl, HONO, HNO<sub>3</sub>, SO<sub>2</sub> and NH<sub>3</sub> and automated IC for on-line analysis.
- Condensed identifier - AWD\_SJAC\_IC : Annular Wet Denuder and Steam Jet Aerosol Collector sampling with on-line IC analysis

Peter McMurry (PM)

University of Minnesota

Four files accepted for permanent storage

EPA\_SS\_ATLANTA\_APM\_TDMA\_PART\_DATA\_1\_PM\_V1.csv

EPA\_SS\_ATLANTA\_APM\_TDMA\_PART\_DATA\_2\_PM\_V1.csv

DMA-APM measurements of particle density

- Condensed identifier - APM\_TDMA : Aerosol Particle Mass Analyzer and Tandem Differential Mobility Analyzer system

EPA\_SS\_ATLANTA\_NANO\_SMPS\_LASAIR\_OPC\_PART\_DATA\_3\_PM\_V1.csv

- DMPS 3: Particle size distributions from 3 nanometers to 3 micrometers
- Condensed identifier - NANO\_SMPS\_SMPS\_LASAIR-OPC : nano Scanning Mobility Particle Spectrometer, Scanning Mobility Particle Spectrometer, Optical Particle Counter

EPA\_SS\_ATLANTA\_TDMA\_PART\_DATA\_4\_PM\_V1.csv

- TDMA measurements of water uptake
- Condensed identifier - TDMA : Tandem Differential Mobility Analyzer system

Paul Solomon (PS)

Environmental Protection Agency

Nine files accepted for permanent storage

EPA\_SS\_ATLANTA\_ASPS\_PART\_DATA\_1\_PS\_V1.csv

EPA\_SS\_ATLANTA\_MOSS\_PART\_DATA\_2\_PS\_V1.csv

EPA\_SS\_ATLANTA\_VAPS\_PART\_DATA\_3\_PS\_V1.csv

EPA\_SS\_ATLANTA\_FRM-A\_PART\_DATA\_4\_PS\_V1.csv

EPA\_SS\_ATLANTA\_FRM-B\_PART\_DATA\_5\_PS\_V1.csv

EPA\_SS\_ATLANTA\_FRM-T\_PART\_DATA\_6\_PS\_V1.csv

EPA\_SS\_ATLANTA\_DICHOT\_PART\_DATA\_7\_PS\_V1.csv

EPA\_SS\_ATLANTA\_SPEC\_PART\_DATA\_8\_PS\_V1.csv

EPA\_SS\_ATLANTA\_URG\_PART\_DATA\_9\_PS\_V1.csv

- 4 types of Speciation Samplers: Andersen, Met One, URG, and VAPS for PM2.5 mass, ions, trace elements, OC/EC
- FRM PM2.5 samplers with Teflon filters for mass and trace elements
- FRM PM2.5 sampler with quartz filter for OC/EC
- Auto Dichotomous sampler with electron microscopy and XRF analysis of fine and coarse PM.
- Condensed identifiers - ASPS : Andersen Speciation Sampler ; MOSS : MetOne Speciation Sampler; VAPS : VAPS Sampler ; FRM-A : FRM Sampler on platform A ; FRM-B : FRM Sampler on platform B; FRM-T : FRM Sampler on roof of trailers; DICHOT : Auto Dichotomous sampler; SPEC : R&P Chemical Speciation Sampler; URG : URG Sampler

Roger Tanner (RT)

TVA Environmental Research Center

One file accepted for permanent storage

EPA\_SS\_ATLANTA\_TVAPC\_BOSS\_PART\_DATA\_1\_RT\_V1.csv

- Particle Concentrator Speciation Sampler BYU Design-Ions and OC/EC data
- Condensed identifier - TVAPC\_BOSS : Particle Concentrator Speciation Sampler BYU Design-Ions and OC/EC data

Rodney Weber and Yin-Nan Lee (RW)

Georgia Institute of Technology and Brookhaven National Laboratory

One file accepted for permanent storage

EPA\_SS\_ATLANTA\_PILS\_IC\_PART\_DATA\_1\_RW\_V1.csv

- CPCIC: CNC-based collection for aerosol ion chromatography for chloride, nitrate, sulfate ammonium ion, sodium, potassium, and calcium.
- Condensed identifier - PILS\_IC : Particle-into-liquid/ion chromatograph

Rod Zika (1 file)

University of Miami

One file accepted for permanent storage

EPA\_SS\_ATLANTA\_OVOC\_PART\_DATA\_1\_RZ\_V1.csv

- On-line GC for volatile organics and oxygenates
- Species measures are: Benzyl Chloride, Freon-12, Freon-114, Chloromethane, Vinyl Chloride, Propylene, 1,3-Butadiene, Bromomethane, Acetaldehyde, Chloroethane, Methanol, Freon-11, Isoprene, 1,1-Dichloroethene, Freon-113, Propanal, Ethanol, Methylene Chloride, Acetone, Hexane, 1,1-Dichloroethane, Methacrolein (MACR), Butanal, Chloroform, 1,1,1-Trichloroethane, Cyclohexane, Methyl Ethyl Ketone (MEK), Carbon Tetrachloride, Benzene, 1,2-Dichloroethane, Heptane, Trichloroethylene, 1,2-Dichloropropane, Pentanal, Bromodichloromethane, 2-Pentanone, trans-1,3-Dichloropropene, Toluene, Methyl Isobutyl Ketone (MIK), cis-1,3-Dichloropropene, 1,1,2-Trichloroethane, Tetrachloroethylene, Dibromochloromethane, 1,2-Dibromoethane, Hexanal, Methyl Butyl Ketone (MBK), Chlorobenzene, Ethylbenzene, o-Xylene, Styrene, Bromoform, a-Pinene, Heptanal, 1,1,2,2-Tetrachloroethane, 4-Ethyltoluene, b-Pinene, 1,3,5-Trimethylbenzene, Benzaldehyde, 1,2,4-Trimethylbenzene, 1,3-Dichlorobenzene, Limonene, 1,4-Dichlorobenzene, Octanal, 1,2-Dichlorobenzene, Nonanal, 1,2,4-Trichlorobenzene, Hexachloro-1,3-Butadiene, Decanal, trans-1,2-Dichloroethene, cis-1,2-Dichloroethene
- Condensed identifier - OVOC : Gas phase Oxygenated Volatile Organic Compounds

Sandy Dasgupta (SD)

Texas Tech University

Four files accepted for permanent storage

EPA\_SS\_ATLANTA\_PPWD\_IC\_GAS\_DATA\_1\_SD\_V1.csv

- Automated IC with continuous parallel plate denuder collection and analysis system for acid gases
- Condensed identifiers - PPWD\_IC : Parallel Plate Wet Denuder / Ion Chromatograph

EPA\_SS\_ATLANTA\_DS\_FIU\_GAS\_DATA\_2\_SD\_V1.csv

EPA\_SS\_ATLANTA\_DS\_FIU\_GAS\_DATA\_3\_SD\_V1.csv

- Semi-continuous HCHO and H<sub>2</sub>O<sub>2</sub> (gas)
- Condensed identifiers - DS\_FLU : Diffusion Scrubber / Fluorescence

EPA\_SS\_ATLANTA\_PCS\_IC\_PART\_DATA\_1\_SD\_V1.csv

- Automated IC with non-water collection system for sulfate, nitrate, nitrite, chloride, and oxalate
- Condensed identifier - PCS\_IC : Filter based Particle Collection System / Ion Chromatograph

Susanne Hering (SH)

Aerosol Dynamics, Inc.

One file accepted for permanent storage

EPA\_SS\_ATLANTA\_ADI\_ICVC\_PART\_DATA\_1\_SH\_V1.csv

- ICVC: Integrated collection and vaporization cell for automated nitrate, sulfate and particulate carbon
- Condensed identifier - ADI\_ICVC : Automated analyze, integrated collection, vaporization cell with NO<sub>x</sub>, SO<sub>2</sub>, and CO<sub>2</sub> detection

Ted Russell (1 file)

Georgia Institute of Technology

One file accepted for permanent storage

EPA\_SS\_ATLANTA\_CFPMM\_TEOM\_PART\_DATA\_1\_TR\_V1.csv

- TEOM: tapered element oscillating microbalance for particle mass, with relative humidity control.
- Condensed identifier - CFPMM\_TEOM : Continuous fine particle mass measurement\_Tapered element oscillating microbalance

### **INTERACTION WITH THE NARSTO QUALITY SYSTEMS SCIENCE CENTER**

A critical part of the archiving activity was the interaction between Georgia Tech and the NARSTO Quality Systems Science Center (QSSC). This collaboration resulted in the discovery of many errors in the data files and the adoption of new keywords.

A typical csv file travels several times between Georgia Tech and the NARSTO QSSC before it is accepted for permanent storage. When a csv file is sent for quality control, a computer program at the QSS center receives the csv file as input. The output from the quality control program consists of a detailed analysis of the csv file where, in many cases, errors or possible errors are indicated. It is useful for the originator of the file to contact personnel at the QSS center to discuss the different warnings and errors issued by the quality control software.

What follows is a sample of warnings and errors that were issued by the quality control software while analyzing some of our files. The error and warning messages have been edited for conciseness. Comments and explanations are also included.

- *Warning, CO-INVESTIGATOR NAME, field number 2 in column C is blank.*

A blank field is not acceptable, if there is not a co-investigator, the key word "Not applicable" should be used.

- *Error, for the variable wind speed another column with identical key characteristics was found.*

The set of key characteristics in each column must be unique. The users should be able to differentiate between two columns based on their characteristics.

- *Warning in key phrase, too many characters.*

A key phrase was used with more than 34 characters.

- *Error, invalid variable type.*

An integer was used within a column defined as character type.

- *Warning, a data gap of 1.15 hours occurs before the date/time 1999/08/09*

The QC program detected a time gap in the measurements. Naturally, the gap could be a valid one.

- *Error, the value 81.3 is flagged M2.*

If 81.3 is a valid value, it can not have a M2 flag that indicates missing value. If the flag M2 is correct, then the value should be -9999.

- *Warning, for date/time 1999/08/11, 14:30, the previous date/time is 4 minutes greater than the date/time start on this record.*

The QC program detected a measurement record out of sequence in time.

- *Warning, the CAS ID C7446-09-5 does not match the variable name Carbon; organic*  
There is a discrepancy between the chemical name and the CAS number.

- *Error, the value 0.3624 is not consistent with the format 8.3*

With four decimal digits, the value 0.3624 corresponds to a format 8.4

- *Warning, variable Voltage is not in the NARSTO lookup table for this key phrase.*

This was one case in which the NARSTO lookup table was updated with the variable "voltage".

- *Warning, for the variable name Temperature, an associated NARSTO standard flag is not present.*

A variable column was defined in such a way that it required an associated column with standard flags.

This process of sending csv files and receiving quality control reports is done until no more errors or warnings are encountered. In some cases, and always in consultation with the QSS center, warning messages are allowed to remain. The time-gap warning (see the fifth example above) is an example of a valid situation in which a warning remains within an accepted file for permanent storage.

## 5.0 Development of the PILS for On-Line Measurements of Aerosol Water Soluble Organic Carbon (WSOC)

In partial support from the Southern Oxidant Study (SOS), an instrument for on-line continuous measurement of the water-soluble organic carbon (WSOC) component of aerosol particles has been developed and deployed at an urban site in St. Louis at the Midwest Supersite. In this method, a Particle-into-Liquid Sampler (PILS) [Orsini *et al.*, 2003; Weber *et al.*, 2001] impacts ambient particles, grown to large water droplets, onto a plate and then washes them into a flow of purified water. The resulting liquid is filtered and the carbon content quantified by a Total Organic Carbon analyzer providing continuous six-minute integral measurements with a detection limit of  $0.1 \mu\text{g C/m}^3$ . From the St Louis study, summer and fall measurements in 2003 of WSOC and organic carbon (OC) indicated WSOC/OC typically ranged from 0.40 to 0.80. A diurnal variation in WSOC/OC that correlated with ozone was observed over extended periods in June; however, other periods in August had no correlation. The results suggested that WSOC was composed of a complex mixture of compounds that may contain a significant fraction from secondary organic aerosol formation. The results from this experiment are summarized in a research paper currently under review [Sullivan *et al.*, 2004]. (This work will comprise a portion of one Georgia Tech graduate student's PhD thesis).

**Diurnal Trends in WSOC and OC at the Midwest Supersite:** As a demonstration of the results from this experiment, diurnal trends in WSOC/OC for PM<sub>2.5</sub> particles are presented.

Our measurements show that for the majority of the time WSOC tracks OC (e.g., for June 2003, hourly-integrated OC regressed on hourly-averaged WSOC yields  $R^2 = 0.81$ ). To further demonstrate the observed behavior, Figure 1 shows the OC concentration, WSOC/OC ratio, and ozone ( $\text{O}_3$ ) concentration for 14-day periods in June and August. A number of interesting features were observed both *within and between these periods*.

The time series for OC revealed a 3-to-7 day trend with a diurnal cycle superposed (EC trends were qualitatively similar to OC trends). The longer-term trend was dictated by precipitation events. Over the multi-day period following a precipitation event (e.g., 6/13/03 and 6/19/03 in Figure 3), the OC increased from approximately  $1\text{-}4 \mu\text{g C/m}^3$  up to about  $10\text{-}15 \mu\text{g C/m}^3$ ; subsequently, the OC concentrations rapidly dropped back to approximately  $1\text{-}4 \mu\text{g C/m}^3$  apparently due to precipitation scavenging. A steady increase in OC concentrations would resume after the rain event. This cycle was observed three times in June 2003 and has the characteristic of a regional buildup of pollution periodically reset by precipitation events. Superposed on this multi-day pattern was a distinct diurnal profile with OC concentration exhibiting a maximum during the night and a minimum during the day. These trends are often observed in urban regions and are indicative of the emissions field being attenuated by atmospheric ventilation with strong vertical mixing during the day and a shallow, stably-stratified mixing layer at night. In contrast, for the period August 1-17 there was no discernable day-to-day buildup in the OC concentration and the aforementioned diurnal profiles were only weakly discernible. October featured a combination of the trends observed for the June and August periods.

WSOC/OC trends also differed between June and August. In June there was a large and consistent variation in the daily WSOC/OC. For extended periods in June, often associated with the aforementioned diurnal OC trends but  $\sim 12$  hours out of phase, there was a clear temporal

pattern in WSOC/OC with levels reaching ~80% during the day and dropping to near 40% at night. In several instances the water-insoluble fraction (WIOC) dominated at night ( $WIOC = OC - WSOC$  and thus  $WIOC/OC = 1 - WSOC/OC$ ). In the past most WSOC measurements have been made using 24-hr integrated filter measurements that are incapable of resolving diurnal variability. The elucidation of sub-daily WSOC patterns and its coupling to OC and other parameters represents a unique observation for an urban site and demonstrates the insights gained from near real-time measurements.

The site was also periodically influenced by strong local point sources. One event can be seen in Figure 3 just prior to midnight on 8/5/03. At this time, the hourly-averaged OC concentration spiked to over  $20 \mu\text{g C}/\text{m}^3$ ; the WSOC concentration, however, did not significantly increase and thus the WSOC/OC ratio was very low (i.e. the water-insoluble OC fraction was high) suggesting that most of the carbonaceous aerosol was likely fresh primary OC.

During the June periods of persistent diurnal trends, the WSOC/OC ratio was fairly well correlated with  $\text{O}_3$ . Table 2 summarizes linear regression results for the entire month of June, and for each period of OC concentration buildup observed between precipitation events. WSOC/OC to  $\text{O}_3$  correlations may suggest that a significant fraction of the June daytime WSOC was associated with SOA. In contrast, diurnal trends in OC and WSOC/OC were not as prominent in August and no correlation was found between WSOC/OC and  $\text{O}_3$  ( $R^2=0.023$ ). The observed contrasts between June and August could be due to a number of factors, including different atmospheric chemical and meteorological processes, and emissions. Thus, significant chemical differences may exist between the WSOC measured in June and August.

Overall, these results show that online measurements of aerosol WSOC, coupled with equally rapid measurements of aerosol OC, provided unique information into the sources and atmospheric processing of fine particulate organic compounds soluble in water. We are currently investigating methods to chemically speciate WSOC online to provide further insights in sources of the organic fraction of fine ambient particles.

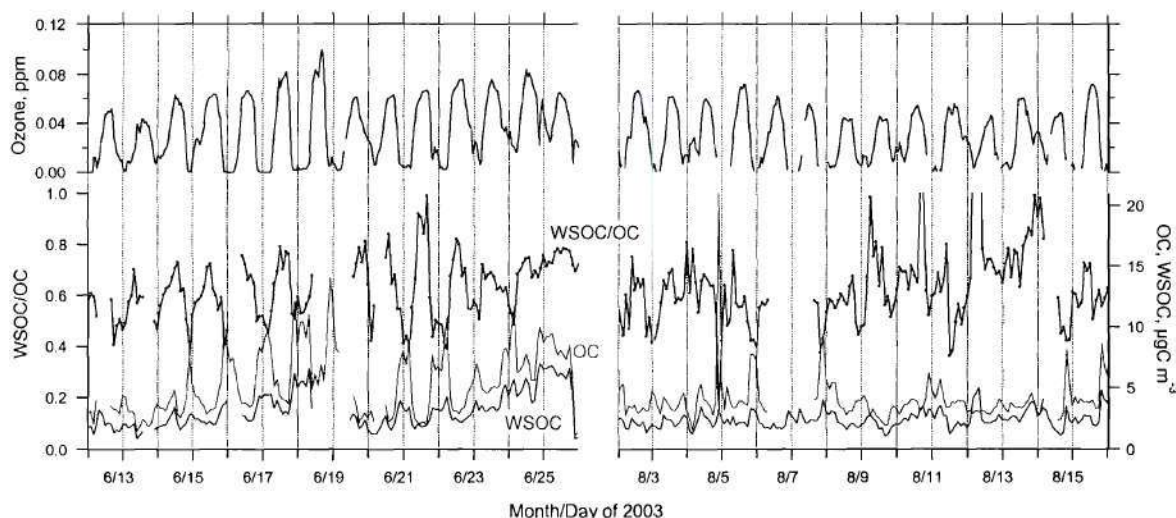


Figure 1. Time series of PM<sub>2.5</sub> OC, WSOC, the fraction of OC that was water-soluble (WSOC/OC), and  $\text{O}_3$  concentration for two 14-day periods in June and August, 2003.

## 6.0 Size-Resolved Water Insoluble Aerosol Concentration in Near Real-Time

The solubility of atmospheric particulate matter influences the hygroscopic growth of particles and thus aerosol chemistry and light extinction properties. Aerosol solubility also affects the ability of particles to create cloud droplets and therefore influences cloud formation and lifetime (and consequently, the radiation balance of the earth). In addition, the dry deposition of insoluble particles to leaf surfaces is believed to negatively influence plant growth and consequently CO<sub>2</sub> uptake. The aerosol water-insoluble fraction is also thought to adversely affect human health. A novel technique to measure the real-time water-insoluble aerosol (WIA) number concentration has been developed at the Georgia Institute of Technology, Atlanta, Georgia. This technique involves the use of a continuous flow impinger with a collection efficiency >90% for particles larger than 0.2  $\mu\text{m}$  and nearly 100% for particles larger than 0.5  $\mu\text{m}$ . A liquid sample stream is continuously pulled from the impinger and passed through a passive debubbling device designed to remove air bubbles created during the impinging process. The total residence time of the impinger and debubbler is less than three minutes. The sample is then passed through a laser particle counter capable of measuring the number concentration of the remaining undissolved particles in fifteen size bins ranging from 0.2  $\mu\text{m}$  to 2.0  $\mu\text{m}$ . The size-resolved number concentration of the total ambient aerosol is measured simultaneously using an ambient optical particle counter. By comparing the insoluble concentration to the total ambient concentration, the size-resolved insoluble fraction may be estimated in near real-time.

Extensive controlled-environment testing of this instrumentation has been conducted at Georgia Tech. This laboratory characterization has demonstrated that the system accurately measures the concentration and size of insoluble polystyrene latex spheres. Publication of these characterization studies is forthcoming. Preliminary field sampling was conducted in August 2002 in Williamson, Georgia in conjunction with the Fall-line Air Quality Study. The WIA instrumentation setup proved to be robust and performed well under field conditions. Figure 1 shows a time series of 30-minute averages of the total and water-insoluble aerosol number concentrations in the size range of 0.3 to 2.0  $\mu\text{m}$ . In January and June, 2003, the instrumentation was used in an intensive air quality study in the alpine region of southeastern France, POVA (Pollution des Vallées Alpines). This campaign consisted of both a winter and summer phase. Figure 2 shows a time series for the winter phase in the Chamonix Valley, and Figure 3 shows a time series for the summer phase at the same location. Figure 4 shows a mass size distribution of both the total and the water-insoluble aerosol populations averaged over the week of data shown in Figure 3. During the winter phase, ambient temperatures were consistently below freezing (a potential problem for an impinger using liquid water). With a few minor modifications, the system behaved reliably. Results from the POVA campaign have already been published in project reports in France and will soon be prepared for peer-reviewed publication. This system has also been used at the facilities of Georgia Tech to characterize WIA concentrations in Atlanta in August and September 2003 and will be used again for the same purposes throughout the summer of 2004.

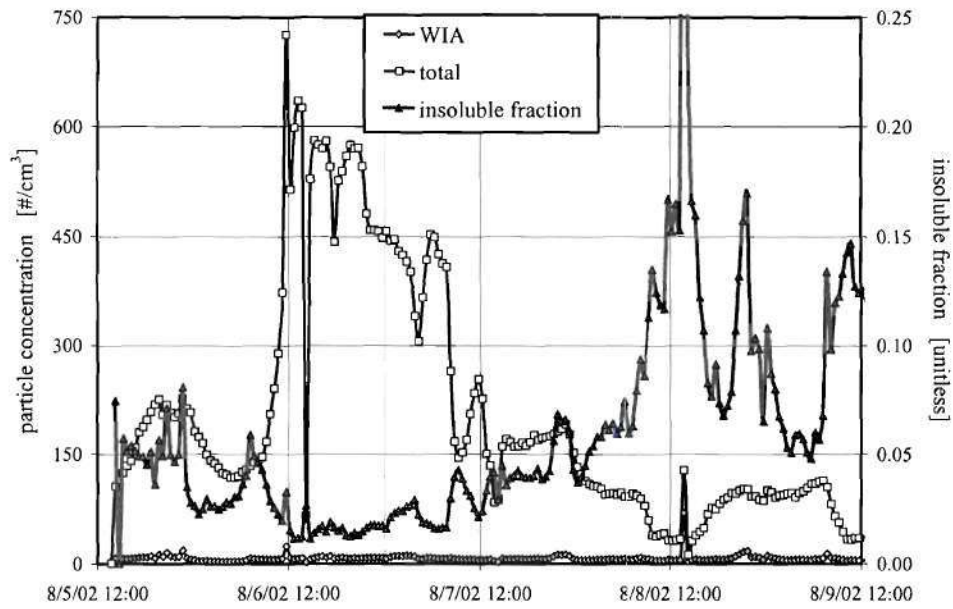


Figure 1: Number concentration at a rural location in central Georgia

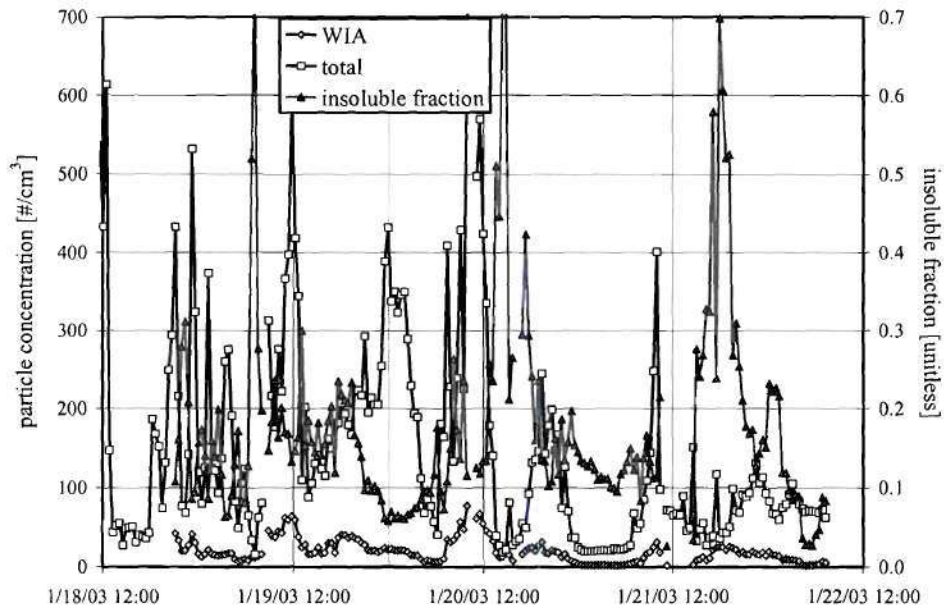


Figure 2: Winter number concentration in the Chamonix Valley

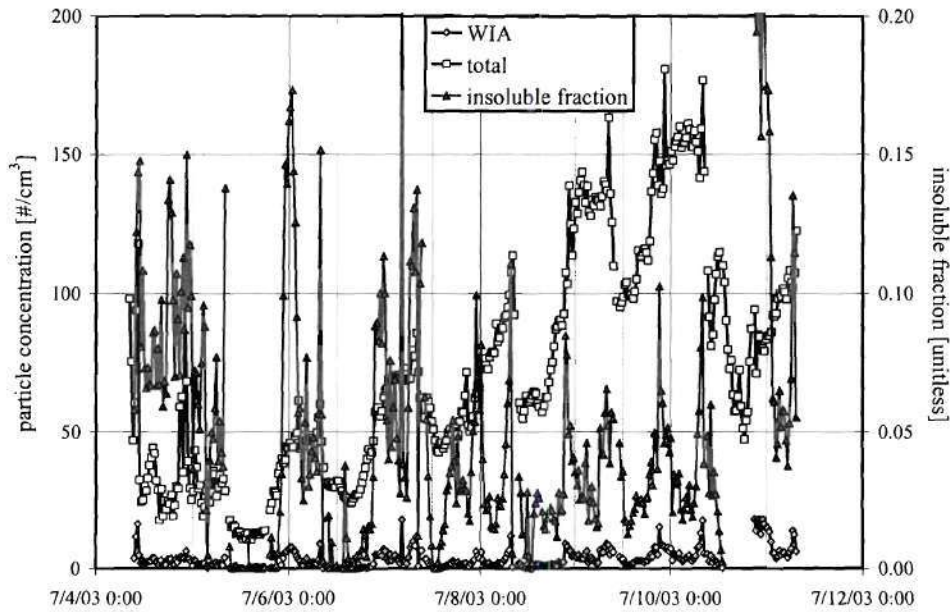
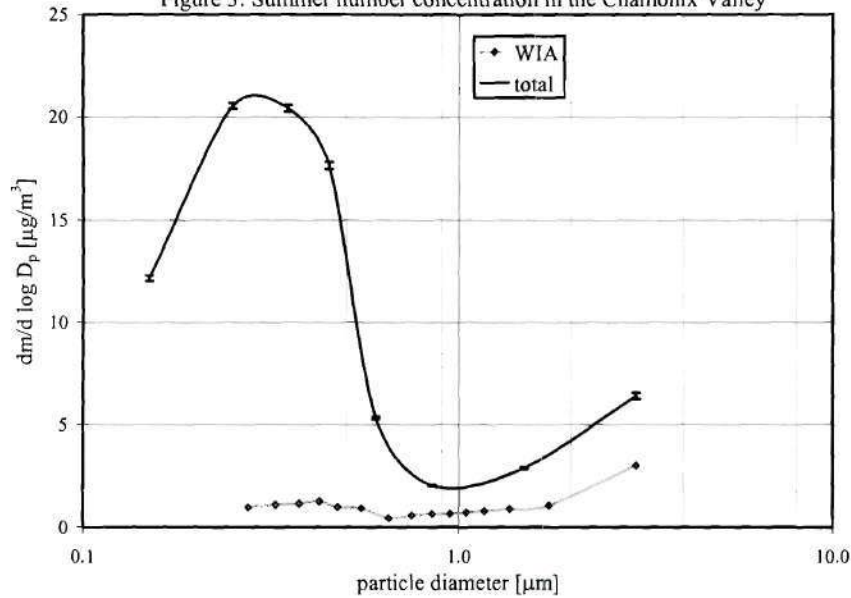


Figure 3: Summer number concentration in the Chamonix Valley



APPENDIX A

SAPRC99 Aerosol Species

ASO4J	-	Accumulation mode sulfate concentration
ASO4I	-	Aitken mode sulfate concentration
ANH4J	-	Accumulation mode ammonium concentration
ANH4I	-	Aitken mode ammonium concentration
ANO3J	-	Accumulation mode nitrate concentration
ANO3I	-	Aitken mode nitrate concentration
AORGAJ	-	Accumulation mode anthropogenic organic concentration
AORGAI	-	Aitken mode anthropogenic organic concentration
AORGPAJ	-	Accumulation mode primary anthropogenic organic concentration
AORGPAI	-	Aitken mode primary anthropogenic organic concentration
AORGBJ	-	Accumulation mode biogenic aerosol concentration
AORGBI	-	Aitken mode biogenic aerosol concentration
AECJ	-	Accumulation mode elemental carbon
AECI	-	Aitken mode elemental carbon
A25J	-	Accumulation mode primary PM2.5 concentration
A25I	-	Aitken mode primary PM2.5 concentration
ACORS	-	Coarse mode anthropogenic aerosol concentration
ASEAS	-	Coarse mode marine aerosol concentration
ASOIL	-	Coarse mode soil-derived aerosol concentration
NUMATKN	-	Aitken mode number
NUMACC	-	Accumulation mode number
SRFATKN	-	Aitken mode surface area
SRFACC	-	Accumulation mode surface area
AH2OJ	-	Accumulation mode water concentration
AH2OI	-	Aitken mode water concentration

APPENDIX B  
Condensable Species

- 1 – ALK (alkanes)
- 2 – OLI1 (alkenes)
- 3 – OLI2 (alkenes)
- 4 – XYL1 (xylenes)
- 5 – XYL2 (xylenes)
- 6 – CSL (cresols)
- 7 – TOL1 (toluenes)
- 8 – TOL2 (toluenes)
- 9 – TRP1 (terpenes)
- 10 – TRP2 (terpenes)

## APPENDIX C

Example of the NARSTO Data Exchange Standard (DES) format and record information.

\*DATA EXCHANGE STANDARD VERSION  
\*QUALITY CONTROL LEVEL  
\*DATE THIS FILE GENERATED/ARCHIVE VERSION NUMBER  
\*ORGANIZATION ACRONYM  
\*ORGANIZATION NAME  
\*STUDY OR NETWORK ACRONYM  
\*STUDY OR NETWORK NAME  
\*FILE CONTENTS DESCRIPTION--SHORT/LONG  
\*PRINCIPAL INVESTIGATOR NAME--LAST/FIRST  
\*PRINCIPAL INVESTIGATOR AFFILIATION  
\*CO-INVESTIGATOR NAME--LAST/FIRST  
\*CO-INVESTIGATOR AFFILIATION  
\*COUNTRY CODE  
\*STATE OR PROVINCE CODE  
\*SAMPLING INTERVAL AS REPORTED IN MAIN TABLE  
\*SAMPLING FREQUENCY OF DATA IN MAIN TABLE  
\*PRINCIPAL INVESTIGATOR CONTACT INFORMATION  
\*DATA USAGE ACKNOWLEDGEMENT  
\*NAME AND AFFILIATION OF PERSON WHO GENERATED THIS FILE  
\*DATE OF LAST MODIFICATION TO DATA IN MAIN TABLE  
\*NAME AND VERSION OF SOFTWARE USED TO CREATE THIS FILE  
\*STANDARD CHARACTERS  
\*COMPANION FILE NAME/FORMAT AND VERSION  
\*TABLE NAME  
\*TABLE FOCUS  
\*TABLE COLUMN NAME  
\*TABLE COLUMN UNITS  
\*TABLE COLUMN FORMAT TYPE  
\*TABLE COLUMN FORMAT FOR DISPLAY  
\*TABLE BEGINS  
    NARSTO standard flags information  
\*TABLE ENDS  
\*TABLE NAME  
\*TABLE FOCUS  
\*TABLE COLUMN NAME  
\*TABLE COLUMN UNITS  
\*TABLE COLUMN FORMAT TYPE  
\*TABLE COLUMN FORMAT FOR DISPLAY  
\*TABLE COLUMN MISSING CODE  
\*TABLE BEGINS  
    Location of monitoring site information  
\*TABLE ENDS  
\*TABLE NAME  
\*TABLE USER NOTE  
\*TABLE FOCUS  
\*TABLE EXPLANATION OF ZERO OR NEGATIVE VALUES  
\*TABLE EXPLANATION OF REPORTED DETECTION LIMIT VALUES  
\*TABLE EXPLANATION OF REPORTED UNCERTAINTY  
\*TABLE USER NOTE2  
\*TABLE KEY FIELD NAMES  
\*TABLE COLUMN NAME  
\*TABLE COLUMN NAME TYPE  
\*TABLE COLUMN CAS IDENTIFIER  
\*TABLE COLUMN USER NOTE  
\*TABLE COLUMN UNITS

\*TABLE COLUMN FORMAT TYPE  
\*TABLE COLUMN FORMAT FOR DISPLAY  
\*TABLE COLUMN MISSING CODE  
\*TABLE COLUMN LOOKUP TABLE NAME  
\*TABLE COLUMN OBSERVATION TYPE  
\*TABLE COLUMN FIELD SAMPLING OR MEASUREMENT PRINCIPLE  
\*TABLE COLUMN PARTICLE DIAMETER--LOWER BOUND (UM)  
\*TABLE COLUMN PARTICLE DIAMETER--UPPER BOUND (UM)  
\*TABLE COLUMN PARTICLE DIAMETER--MEDIAN (UM)  
\*TABLE COLUMN MEDIUM  
\*TABLE COLUMN COATING OR ABSORBING SOLUTION/MEDIA  
\*TABLE COLUMN WAVELENGTH (NM)  
\*TABLE COLUMN INLET TYPE  
\*TABLE COLUMN SAMPLING HUMIDITY OR TEMPERATURE CONTROL  
\*TABLE COLUMN LABORATORY ANALYTICAL METHOD  
\*TABLE COLUMN SAMPLE PREPARATION  
\*TABLE COLUMN BLANK CORRECTION  
\*TABLE COLUMN VOLUME STANDARDIZATION  
\*TABLE COLUMN INSTRUMENT NAME AND MODEL NUMBER  
\*TABLE COLUMN DETECTION LIMIT  
\*TABLE BEGINS  
    Data  
\*TABLE ENDS

## REFERENCES

- Christensen, S.W., Boden, T.A., Hook, L.A., and Cheng, M-D., "NARSTO Data Management Handbook", NARSTO Quality Systems Science Center, Environmental Sciences Division, Publication No. 4917, Oak Ridge National Laboratory, Oak Ridge, Tennessee, February 2000.
- Orsini, D., Y. Ma, A. Sullivan, B. Sierau, K. Baumann, and R. Weber, Refinements to the Particle-Into-Liquid Sampler (Pils) For Ground and Airborne Measurements Of Water Soluble Aerosol Composition, *Atm. Environ.*, 37, 1243-1259, 2003.
- Sullivan, A.P., R. J. Weber, A.L. Clements, J.R. Turner, M.S. Bae, and J.J. Schauer, A method for on-line measurement of water-soluble organic carbon in ambient aerosol particles: Results from an urban site, *Geophys. Res. Lett.*, in review, 2004.
- Weber, R.J., D. Orsini, Y. Daun, Y.-N. Lee, P. Klotz, and F. Brechtel, A particle-into-liquid collector for rapid measurements of aerosol chemical composition, *Aerosol Sci. Tech.*, 35, 718-727, 2001.
- Boylan, JW, Odman, MT, Wilkinson, JG, Russell, AG, Doty, K., Norris, W. and McNider, R. Development of a comprehensive multiscale "one atmosphere" modeling system: Application to the southern Appalachian mountains. *Atmospheric Environment*, 36 (23): 3721-3734., 2002
- Cohan, D.S., Hu, Y., Hakami, A., Odman, M.T., Russell, A.G.,  
Implementation of a direct decoupled sensitivity method into CMAQ. 1st Models-3 Users Workshop. [www.cmascenter.org/workshop/session5/cohan\\_abstract.pdf](http://www.cmascenter.org/workshop/session5/cohan_abstract.pdf). 2002.
- Nenes A., Pilinis C. and Pandis S.N. (1998) ISORROPIA: A new thermodynamic equilibrium model for multiphase multicomponent inorganic aerosols. *Aquatic Geochemistry*. 4., 123-152.

### **Publications with support full or in part by the SOS Cooperative Agreement**

- Biazar, A., R. McNider, S. Roselle, S. Haines, G. Jedlovec, R. Suggs, D. Byun, S. Kim, 2004: Assimilation of GOES satellite data in CMAQ: Correcting photolysis rates based on observed clouds. To be submitted *J. Geophysical Research*.
- Herwehe, J., R. McNider, A. Biazar, W. Norris. Initial application of a coupled LES-photochemical model to examine near-source ozone production from industrial emissions. *Symposium on Turbulence and Diffusion, American Meteorological Society, Wageningen, Netherlands, July 2002*.
- McNider, Richard T., W. Lapenta, A. Biazar, G. Jedlovec, J. Pliem, 2004: Retrieval of model grid scale heat capacities using geostationary satellite products. To be submitted *J. Applied Meteor.*
- McNider, R., W. Norris, A. Biazar, 2004: Role of deformation zones in producing extreme concentration events. To be submitted to *Science Magazine*.

Sang-Ok Han, Arastoo Pour Biazar, Richard McNider, John Nielsen-Gammon, William Lapenta, Kevin Doty, and Stephanie L. Haines., 2004: Assimilation of GOES IR data for urban meteorological modeling: evaluation of the importance of sub-grid inhomogeneity. : *Symposium on Planning, Nowcasting, and Forecasting in the Urban Zone, American Meteorological Society, January, 2004.*

Xhi, S., R. McNider, M. Friedman, D. England, W. Norris, M.P. Singh, 2004: On the behavior of the stable boundary layer and role of initial conditions. *Accepted Pure and Applied Geophysics (PAGEOPH).*

Zamora, R. J., S. Solomon, E. G. Dutton, J. W. Bao, M. Trainer, R. W. Portmann, A. B. White, D. W. Nelson, and R. T. McNider, 2002: Comparing MM5 radiative fluxes with observations gathered during the 1995 and 1999 Nashville Southern Oxidants Studies. *J. of Geophys. Res.*,**108**, ACL9-1-ACL 9-13.